Performance Comparison of R-PHY and R-MACPHY Modular Cable Access Network Architectures

Ziyad Alharbi, Akhilesh S. Thyagaturu, Martin Reisslein, *Fellow, IEEE*, Hesham ElBakoury, and Ruobin Zheng

***Abstract*—Emerging modular cable network architectures distribute some cable headend functions to remote nodes that are located close to the broadcast cable links reaching the cable modems (CMs) in the subscriber homes and businesses. In the remote-PHY (R-PHY) architecture, an R-PHY device conducts the physical layer processing for the analog cable transmissions, while the headend runs the data over cable service interface specification (DOCSIS) medium access control (MAC) for the upstream transmissions of the distributed CMs over the shared cable link. In contrast, in the remote MACPHY (R-MACPHY) architecture, an R-MACPHY device (RMD) conducts both the physical and MAC layer processing. In this paper, we conduct a comprehensive performance comparison of the R-PHY and R-MACPHY architectures. We first develop analytical delay models for the polling-based MAC with gated bandwidth allocation of Poisson traffic in the R-PHY and R-MACPHY architectures. We then conduct extensive simulations to assess the accuracy of the analytical model and to evaluate the delay-throughput performance of the R-PHY and R-MACPHY architectures for a wide range of deployment and operating scenarios. Our evaluations include long converged interconnect network (CIN) distances between remote nodes and headend, bursty self-similar traffic, and double-phase polling to mask long CIN propagation distances. We find that for long CIN distances above 100 miles, the R-MACPHY architecture achieves significantly shorter mean upstream packet delays than the R-PHY architecture, especially for bursty traffic. Our extensive comparative R-PHY and R-MACPHY evaluation can serve as a basis for the planning of modular broadcast cable based access networks.**

***Index Terms*—Broadcast cable, delay, DOCSIS, Internet access, medium access control, polling.**

Manuscript received February 23, 2017; revised May 14, 2017; accepted May 24, 2017. Date of publication June 27, 2017; date of current version March 2, 2018. This work was supported by Huawei Technologies Company Ltd. *(Corresponding author: Martin Reisslein.)*

Z. Alharbi, A. Thyagaturu, and M. Reisslein are with the School of Electrical, Computer, and Energy Engineering, Arizona State University, Tempe, AZ 85287-5706 USA (e-mail: zalharbi@asu.edu; athyagat@asu.edu; reisslein@asu.edu).

H. ElBakoury is with Futurewei Technologies Inc., 2330 Central Expressway, Santa Clara, CA 95050 USA (e-mail: hesham.elbakoury@huawei.com).

R. Zheng is with the Fixed Network Research Department, Huawei Technologies Company Ltd., Shenzhen, Guangdong 518129, China (e-mail: zhengruobin@huawei.com).

Color versions of one or more of the figures in this paper are available online at http://ieeexplore.ieee.org.

Digital Object Identifier 10.1109/TBC.2017.2711145

I. Introduction

A. Motivation

CABLE networks were traditionally designed to carry broadcast television (TV) to a large number of households. However, as the demand for unicast Internet services increased, Cable Modems (CMs) and the Data Over Cable Service Interface Specification (DOCSIS) were introduced to transmit unicast data over the shared broadcast channel in a cable network. Advances in cable technologies have enabled Internet speeds up to 1 Gbps in both the uplink and downlink direction to each CM.

As a result, multi-system operators that operate multiple cable TV systems see unprecedented opportunities for the development of innovative techniques that utilize the already deployed cable infrastructures so as to meet present and future Internet connectivity demands. However, the traditional cable network elements were not developed to be flexible, resulting in increased capital and operational expenditures (CAPEX/OPEX) for installing new infrastructures and upgrading existing infrastructures as technologies advance. Recently, numerous techniques have been proposed to reduce the costs, such as the converged cable access platform (CCAP) and the modular Cable Modem Termination System (CMTS), see Section II-A and [1]–[4].

In order to reduce the propagation distances of analog signals in these broadcast cable based Internet access systems there has been a trend to modularize the cable headend processing. Digital signals are then transmitted to the headend processing modules that are distributed to remote nodes placed in close proximity to the CMs; thus analog signals travel only short distances from the headend processing modules in remote nodes to the CMs. Two main competing strategies have recently been proposed: Remote-PHY (R-PHY), where the physical layer processing for the cable transmission is conducted in distributed remote nodes while the medium access control (MAC) is conducted in a centralized headend location, and Remote MACPHY (R-MACPHY) [2], [3], [5], [6], where both physical layer and MAC processing are conducted in remote nodes.

B. Related Work

Access networks based on broadcast cable have been extensively studied during the development of the IEEE 801.14 protocol mechanisms, see [7]–[15], which subsequently

influenced the DOCSIS specification [16]–[18]. Several studies have evaluated and refined the basic DOCSIS mechanisms. Simulation models for DOCSIS have been developed in [19]–[21], while the upstream throughput of DOCSIS 1.1 has been examined in [22]–[25], and the transmission of MPEG and IPTV video on DOCSIS has been considered in [26]–[28]. Initial dynamic bandwidth allocation (DBA) designs for Quality of Service (QoS) based grant allocations have been discussed in [29]. A CM can content with other CMs for the upstream transmissions of request messages to the CMTS at the headend. The DOCSIS contention behavior has been examined in [30]–[35]. In order to resolve the contention, Kuo *et al.* [36] have presented a priority access based collision resolution scheme for different traffic priorities. Similarly, Heyaime-Duvergé and Prabhu [37] have proposed an application traffic based DBA to reduce the control signaling and increase bandwidth utilization. As an improvement to the earlier DOCSIS versions, Liao and Ju [38] and Liao [39] proposed to adaptively allocate the TCP flow transmission slots by using fast request transmission and long packet deferment techniques. The impacts of the DOCSIS MAC protocols on TCP have been further investigated in [40]. DOCSIS simulation models have been presented in [19], [21], and [41]. All of these prior studies have considered conventional cable access architectures where all headend functions are co-located in the headend.

In contrast, we examine modular cable access architectures in this study, where some headend functions are distributed to remote nodes. Prior studies on modular cable access network architectures have mostly been qualitative in nature, exploring the various features and possibilities opened up by modularizing the cable headend [4], [42]–[45] We are only aware of one prior quantitative study on modular cable network architectures, namely the study by Chapman *et al.* [46]. Chapman *et al.* [46] have presented a preliminary performance analysis of the impact of the CIN distance from the remote node to the headend (CCAP core) in the R-PHY architecture for Poisson traffic. In contrast, we provide a comprehensive performance evaluation of both the R-PHY and R-MACPHY modular cable architectures for both Poisson and bursty self-similar traffic.

The cable DOCSIS MAC protocol is based on the general polling strategy [47]–[49], which has been mathematically analyzed in various other network contexts, such as passive optical access networks, see [50]–[58]. Most mathematical analysis work for cable access networks has focused on the contention of bandwidth requests, see for instance [30]–[36]. Complementary to these existing mathematical analyses of the bandwidth request contention in cable access networks, we consider the piggybacking of bandwidth requests on upstream data transmissions [59] and focus on the polling MAC dynamics. Specifically, we adapt existing delay analysis strategies for polling to the cable DOCSIS MAC protocol.

C. Contributions

This article makes two main original contributions to the research on access networks based on broadcast cable networks. First, we adapt mathematical models of polling based medium access control to mathematically analyze the mean upstream data packet delay in cable access networks. In particular, we develop delay models for the R-PHY and R-MACPHY modular cable architectures. That is, we develop delay models for the R-PHY architecture, which makes upstream MAC decisions in the headend, as well as the R-MACPHY architecture, which makes MAC decisions in the remote nodes.

Second, we conduct an extensive numerical comparison of the throughput-delay performance of the R-PHY and R-MACPHY architectures for a wide range of scenarios. We examine traffic burstiness levels ranging from Poisson traffic to highly bursty self-similar traffic. We consider CIN network distances ranging from tens of miles to 2000 miles, which may arise when conducting the DOCSIS MAC processing in a headend that is virtualized in the cloud. We consider dynamic bandwidth allocation based on Gated grant sizing and Excess sharing grant sizing in combination with offline and double-phase polling (DPP) scheduling, which closely approximates pipelined scheduling.

TABLE I
SUMMARY OF MAIN ACRONYMS

CCAP	Converged Cable Access Platform (CCAP core implements CMTS headend functions)
CIN	Converged Interconnect Network (between RN and CMTS)
CM	Cable Modem
CMTS	Cable Modem Termination System (DOCSIS cable headend)
DEPI	Downstream External PHY Interface (downstream CCAP core to RPD PWs)
DOCSIS	Data Over Cable Service Interface Specification
MAP	Bandwidth Allocation MAP
PW	Pseudowire (logical link between RN and CCAP core)
RMD	Remote MACPHY Device
RN	Remote Node (either RMD or RPD)
RPD	Remote PHY Device
SG	Service Group (group of CMs)
UEPI	Upstream External PHY Interface (upstream RPD to CCAP core PWs)
vMAC	virtual MAC (implemented in cloud)

D. Organization

Throughout this article, we compare the R-PHY and R-MACPHY modular architectures of access networks based on the broadcast cable medium. Towards this end, this article is organized as follows:

1) Overviews of the architectural and protocol concepts of R-PHY and R-MACPHY are given in Sections II and III.
2) The end-to-end upstream mean packet delays in the R-PHY and R-MACPHY architectures are analytically modeled in Section IV.
3) Numerical performance comparisons based on analytical and simulation results for a wide range of cable network parameters are presented in Section V.

The main acronyms used in this article are summarized in Table I.

II. BACKGROUND ON DISTRIBUTED CABLE ACCESS ARCHITECTURES

A. General Background on Cable Access Networks

1) Converged Cable Access Platform (CCAP): The Converged Cable Access Platform (CCAP) integrates the physical layer QAM modulators [60] for video and data into an

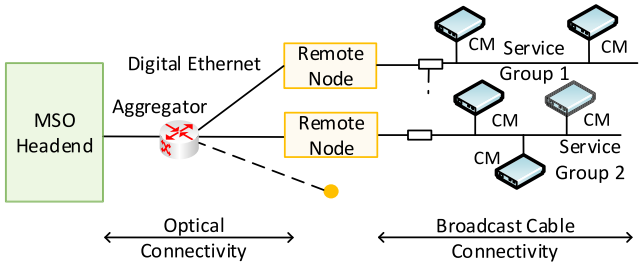

Fig. 1. The modular headend version 2 (MHAv2) architecture moves some CCAP functions from the headend to the remote nodes. The remote nodes are typically connected to the Headend/CCAP core via a digital Ethernet fiber network. In the Remote-PHY (R-PHY) architecture, the remote node implements the DOCSIS PHY. In the Remote-MACPHY (R-MACPHY) architecture, the remote node implements both DOCSIS PHY and MAC. The R-PHY and R-MACPHY nodes serve the attached cable access networks in broadcast mode.

universal QAM for DOCSIS connectivity to the CMs. DOCSIS specifies the MAC [19] and PHY layers for communication between the distributed CMs and the central cable modem termination system (CMTS) at the headend. Traditionally, hybrid fiber coax access networks [61], [62] used analog optical transceivers at the headend to generate amplitude modulated analog optical signals to carry the information over a fiber to a remote analog fiber node which converted the optical signals to radio frequency (RF) signals for transmission over the coaxial cable to the CMs. Limitations of analog transmissions have motivated the development of modular headend architectures with digital transmission over the fiber segment from headend to remote node.

2) Modular Headend Architecture (MHA): The Modular Headend Architecture (MHA) modularizes the CCAP network functions so that the network functions can be distributed among (split between) headend and remote nodes, whereby the headend and remote nodes are connected by a digital fiber, as illustrated in Fig. 1. Digital fiber supports long distance transmissions and variants of the 802.3 family of Ethernet protocols, such as Ethernet Passive Optical Networks (EPONs, IEEE 802.3ah, IEEE 802.3av). A secure Layer 2 Ethernet or PON link over a digital fiber connects the remote node to the headend through multiple logical or physical channels, thus forming a digital fiber coax network to the attached CMs [63]. Implementing some CCAP functions in remote nodes near the CMs reduces the analog transmission distances, thus improving the signal to noise ratio at the CMs [64].

Typically, a remote node is located outdoors as a pole-mounted fiber node or remote cabinet and transfers DOCSIS frames between an IP network interface and an RF interface. The centralized functions can be physically implemented in the headend; however, they can also be implemented at a remote site beyond the headend, e.g., in a regional datacenter or in the cloud. The CCAP core at the headend typically consists of all the traditional CMTS function, except for functions implemented at the remote nodes. The network between the CCAP core and the remote node can contain both Layer 2 switches and Layer 3 routers and is commonly referred to as the Converged Interconnect Network (CIN) [65].

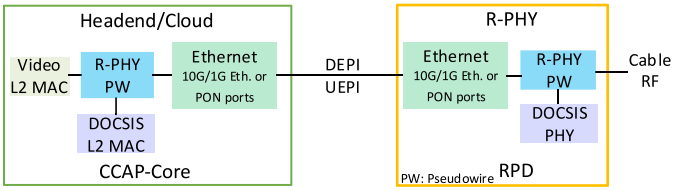

Fig. 2. R-PHY architecture: DOCSIS MAC is implemented at the CCAP core, whereas, the DOCSIS PHY is implemented at a Remote-PHY Device (RPD).

B. Remote PHY (R-PHY) Architecture

The Remote-PHY (R-PHY) [5] architecture implements the DOCSIS PHY layer at the remote node, whereas the DOCSIS upper layers and MAC are centrally implemented at the headend or cloud. More specifically, the R-PHY architecture separates the DOCSIS PHY functions from the traditional CCAP chassis. Separating functions in the CCAP platform can achieve several benefits, such as independent scaling of MPEG video delivery, and flexible management of DOCSIS and out-of-band (OOB) cable transmissions. OOB transmissions use the frequency bands that are mutually exclusive to the bands reserved for the traditional data transmissions. OOB provides auxiliary services, such as Set Top Box (STB) connectivity and management in cable access platforms [66]. The function separation in the CCAP platform makes the software and physical hardware upgrades in the R-PHY architecture modular and independent, resulting in improved availability and manageability [42], [45].

1) R-PHY Internals: The R-PHY architecture separates the CCAP into CCAP core functions that are implemented at a centralized location (e.g., headend or cloud), and into DOCSIS PHY functions that are implemented at the RPD, as shown in Fig. 2. The CCAP core in an R-PHY architecture consists of the CMTS for DOCSIS (which in turn consists of the DOCSIS MAC and upper layers) and an edge QAM (EQAM) [62] MAC for video. The DOCSIS upper layers include control signaling functions, downstream and upstream bandwidth schedulers, as well as DOCSIS framing. The RPD connects to the CCAP core through a network interface and connects to the CMs through an RF interface. An RPD also supports the Layer 1 PHY conversion, Layer 2 MAC conversion, and Layer 3 pseudowires (PWs) [5]. An IP PW is a logical interface, such as an IP tunnel, that seamlessly transports the DOCSIS frames between the CCAP core and the RPD.

The RPD receives the downstream DOCSIS signals from the CCAP core over a digital medium, such as Ethernet or PON. The RPD then essentially functions as a physical layer converter that converts the received digital signals to analog signals for RF transmissions over the coaxial cable. In the upstream direction, the RPD converts the DOCSIS analog signals received from the CMs of a service group (SG) to digital frames. These digital frames are then transported to the CCAP core at the headend/cloud for further processing.

2) R-PHY Transport Mechanisms: The Downstream External PHY Interface (DEPI) [67] and Upstream External PHY Interface (UEPI) [68] provide the transport mechanisms between the RPD and the CCAP core. DEPI and UEPI are

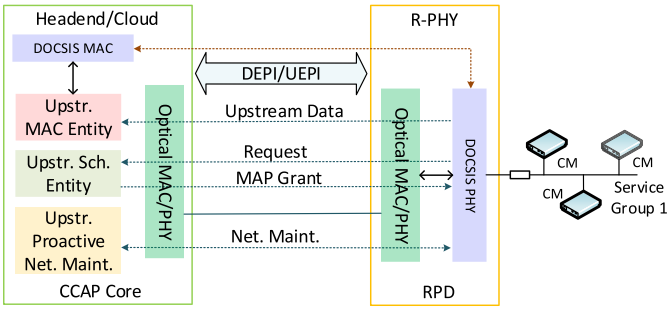

Fig. 3. DEPI and UEPI protocol mechanisms create multiple pseudowires (PWs) between CCAP core and RPD to transport the DOCSIS PHY frames in the downstream and MAC frames in upstream directions.

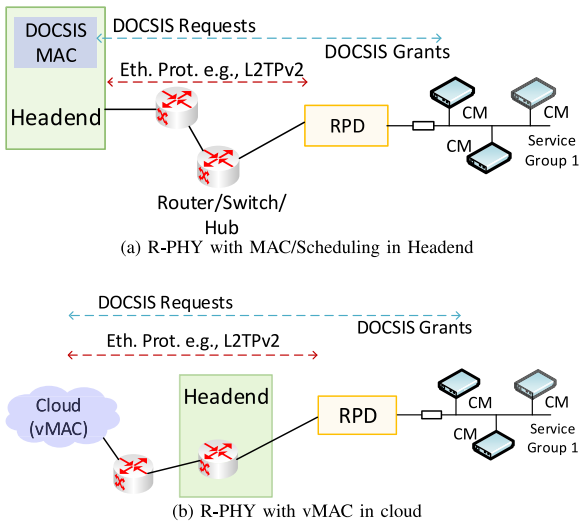

Fig. 4. (a) R-PHY with Ethernet CIN and MAC/Scheduling in Headend (Section II-B3a): Ethernet links provide the CIN connectivity between the RPD and headend. The CCAP core is located at the headend and implements the DOCSIS MAC and scheduling. (b) R-PHY with Ethernet CIN and vMAC in cloud (Section II-B3b): DOCSIS MAC and scheduling are implemented at a cloud location. An Ethernet connection spans from the cloud to the RPD, enabling the communication between DOCSIS vMAC and RPD.

based on the Layer 2 Tunneling Protocol version 3 (L2TPv3), i.e., RFC 3931 [69]. The L2TPv3 transparently transports Layer 2 protocols over a Layer 3 network creating the PWs. As illustrated in Fig. 3, the DEPI consists of multiple PWs between the DOCSIS MAC module at the CCAP core and the PHY module in the RPD so as to create independent paths for signalling and data transmissions between RPD and CCAP core. The signalling transmissions include control frames for setting up, maintaining, and tearing down of sessions. The data transmissions include DOCSIS data frames, video packets, and OOB packets. In addition, the DEPI supports the Packet Streaming Protocol (PSP) [70] for advanced services, such as DOCSIS 3.1. Similar to DEPI, the UEPI also creates PWs between the CCAP core and RPD, supporting independent control and data transmissions in the upstream direction.

More specifically, the downstream operation at the RPD involves DOCSIS framing of the payloads that are extracted from the traffic received by the DEPI interface, the RF modulation of DOCSIS frames, and the RF signal transmissions over the cable interface. When the signal is received from the coax cable in the upstream direction, the operations at the R-PHY include the RF demodulation, the digitization of the received analog RF signals, and the extraction of DOCSIS frames. The resulting frames are then encapsulated by the UEPI for transmissions via the network interface to the CCAP core. In order to support the DOCSIS MAC, the RPD extracts the bandwidth requests from the DOCSIS frames that arrive from the CMs. The RPD then encapsulates and sends the requests with priority over a separate PW. In particular, the routers and switches in the CIN support Differentiated Services Code Points (DSCPs) and can be configured with Per Hop Behaviors (PHBs) [71] such that control signalling traffic is prioritized. That is, the DOCSIS control packet traffic is forwarded with priority to achieve low latency while traversing the CIN [72].

3) R-PHY Variants: The CIN network between CCAP core and RPD is typically either an active Ethernet network or an optical network. The DOCSIS MAC can be implemented either at the headend (i.e., CCAP core) or in remote data centers (i.e., cloud). Additionally, the DOCSIS scheduler can be implemented either at the headend or RPD, i.e., the scheduler could be separated from the MAC [5, Sec. 10.1, Annex B1]. Thus, a variety of combinations of CIN type, vMAC location, and DOCSIS scheduler location are possible. We consider the DOCSIS MAC and scheduler to be co-located throughout. More specifically, we focus in this study on two common variants of R-PHY with Ethernet CIN: *i*) DOCSIS MAC and scheduling in the headend, and *ii*) DOCSIS MAC and scheduling implemented in the cloud (vMAC).

a) R-PHY with Ethernet CIN and MAC/scheduling in headend: This R-PHY with Ethernet variant connects the RPD with the CCAP core through IEEE 802.3 [73] links over switches and routers in the CIN. The CCAP core implements the DOCSIS MAC and scheduler in the headend as show in Fig. 4(a). DEPI and UEPI interfaces establish the L2TPv3 tunnels so that the DOCSIS request (REQ) and grant (GNT) control messages traverse the CIN between the CCAP core at the headend and the RPD over prioritized L2TPv2 sessions.

b) R-PHY with Ethernet CIN and cloud vMAC: The virtualization of the DOCSIS MAC and scheduling in a cloud vMAC effectively shifts the MAC and scheduling implementation to a remote datacenter or cloud. Therefore, the DEPI and UEPI sessions are established between the cloud location and the RPD, as illustrated in Fig. 4(b). The headend functions as a switch or router supporting the L2TPv3 mechanisms. The DOCSIS REQ and GNT messages traverse all the way between the remote cloud location and the RPD, resulting in longer request-grant delay compared to an R-PHY with DOCSIS MAC and scheduler at the headend.

C. Remote-MACPHY (R-MACPHY) Architecture

The Remote-MACPHY (R-MACPHY) architecture moves both the DOCSIS MAC and PHY layers out to the remote node, which is referred to as Remote MACPHY Device (RMD) [74]. The connection between the CCAP core and the RMD is essentially a Layer 2 Ethernet connection. In the downstream direction, an RMD accepts data from a headend

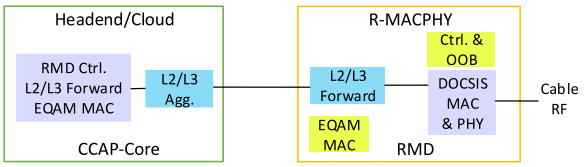

Fig. 5. Illustration of R-MACPHY Architecture: DOCSIS MAC and PHY are implemented at the Remote MACPHY Device (RMD). The upper DOCSIS layers are implemented at the headend.

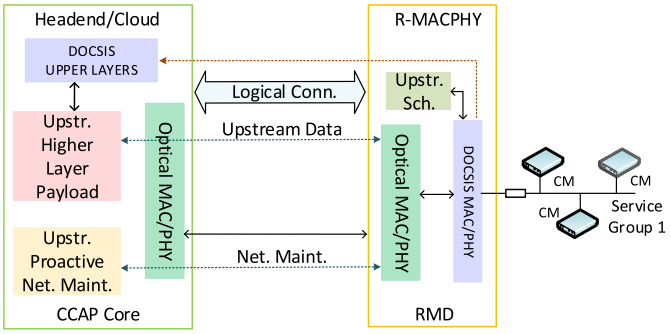

Fig. 6. A generic interface can be used to transport the DOCSIS upper layer data from RMD to DOCSIS upper layers, which are implemented at the CCAP core headend.

L2 aggregation device, i.e., the RMD accepts data, video, and digitized signal sequences from an external OOB converter [3]. In the upstream direction, the RMD collects data from cable modems and set-top boxes (STBs), and forwards the data to the headend and STB control system. Thus, the RMD transparently converts the optical data frames on the headend-to-RMD network to RF data frames on the broadcast cable network and vice versa.

The R-MACPHY design can vary based on the implementation of the remaining CCAP functions, i.e., the CCAP functions that do not belong to DOCSIS CMTS MAC and PHY. These remaining CCAP functions can be either implemented at the headend or in the cloud. Common to all design variants is that the MAC and PHY are implemented on the same RMD physical device.

1) R-MACPHY Internals: Figure 5 highlights the components that are common to the variety of options. Distributed architectural variations of R-MACPHY can be mainly classified into: *i*) RMD with minimal configuration, i.e., only the DOCSIS MAC is implemented at the RMD, *ii*) RMD with embedded edge-QAM (EQAM) [62], i.e., the MAC for both video and DOCSIS data are implemented at the RMD, *iii*) Remote CCAP (R-CCAP), which implements all CCAP functions at the remote nodes, and *iv*) R-CCAP with centralized controller. Our evaluation considers the implementation of the MAC scheduler at the remote node, which is common to the variations of the R-MACPHY architecture.

2) R-MACPHY Transport Mechanisms: With the DOCSIS MAC implemented at the RMD, only the upper layer (i.e., L3 and above) DOCSIS data must be transported to the CCAP core located at the headend for further processing. The request-grant delay is much shorter compared to R-PHY, since the exchange of REQ and GNT messages occurs over much shorter distances, namely between RMD and CMs. While the

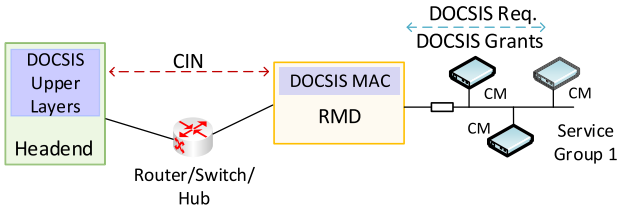

Fig. 7. DOCSIS request and grant messages are exchanged over coaxial cable between Remote-MACPHY Device (RMD) and CM.

RPD in the R-PHY architecture must prioritize the REQ packet transmissions over normal payload data traffic on the CIN, the RMD does not require any such prioritization.

Typically, the headend and RMD are connected through a Layer 2 digital transport connection over optical fiber. Thus, RMD traffic can be transported by optical Gigabit Ethernet CINs or EPON/GPON CINs [75]. Logical connections, such as L2/L3 tunnels (interfaces) provide transparent flow level connections between RMD and headend, as described in Fig. 6.

3) R-MACPHY With Ethernet CIN: An Ethernet CIN composed of routers and switches can interconnect the RMD and the headend, e.g., the CIN in Figure 7 is composed of an active Ethernet network. The RMD essentially forwards the L2/L3 packets to the CCAP core. A layer 2 or 3 level connection, such as Layer 2 Virtual Private Network (L2VPN) or L2TPv3 is established between the RMD and headend.

III. Distributed Cable Access Protocols

DOCSIS implements a centralized reservation-based allocation of the cable upstream bandwidth for the CM transmissions. Periodically, the headend sends a bandwidth allocation MAP (MAP) to inform attached CMs of the start time and duration of their next upstream transmission windows. Also, the allocation MAP defines the slots available for contention transmission and the slots available for new CMs to join the network [20]. More specifically, CMs can acquire bandwidth for upstream data transmission through requests sent with contention or with piggybacking onto data transmissions. Piggybacking avoids contentions, since the requests are transmitted along with the upstream payload data [37].

A. Background on Dynamic Bandwidth Allocation

We categorize and identify the dynamic bandwidth allocation (DBA) algorithms in the polling based DOCSIS MAC protocol using the three design dimensions, i) grant scheduling framework which characterizes the event triggering the scheduling and bandwidth allocation as well as the overall structure of the granting and scheduling process, ii) grant sizing policy which determines the size of the upstream transmission window allocated to each CM, and iii) grant scheduling policy which arranges the order of the different scheduled transmission windows [76]–[79]. A dynamic bandwidth allocation (DBA) algorithm in the DOCSIS scheduler sizes (dimensions) the upstream transmission windows (grants) based on the reports received by the CMs and sends the grants via MAP messages to the respective CMs.

1) Grant Scheduling Framework:

a) Offline: Grant transmission windows are allocated after REPORTs from all CMs have been received at the CMTS. That is, the schedule for the entire granting cycle of CM upstream transmissions is generated when the REPORT message from the last CM is received.

b) Double phase polling (DPP): CMs in a SG are partitioned into two independent DPP groups. Within each DPP group, the granting and scheduling is triggered by the receipt of REPORTs from all CMs in the group. Each DPP group is scheduled independently in an offline manner.

2) Grant Sizing Policy: In DOCSIS 3.1, grant sizes are allocated to the CMs in terms of number of minislots. Each minislot corresponds to a set of specific frequency subcarriers for a specific transmission time duration. An OFDM symbol is the fundamental unit of the minislot, and the number of OFDM symbols for each minislot in a given SG is defined as per the specifications in [59]. The grant sizing policy determines the grant sizes in terms of minislots such that the CM transmissions are orthogonal. By maintaining orthogonality, each CM gets exclusive access (without collisions) to the cable broadcast channel for its upstream transmissions. Effectively, a group of minislots that are reserved for the transmissions of a given CM can be abstracted to a variable transmission (bandwidth) bitrate channel.

The grant sizing policy determines the transmission window size (in terms of number of OFDM minislots) based on the CM upstream transmission request (in terms of bytes of data queued for upstream transmission). We consider two widely considered grant sizing policies for the comparison of the R-PHY and R-MACPHY architectures:

a) Gated: The Gated grant sizing mechanism grants the CMs their full amount of requested bandwidth [76], [79]–[81].

b) Limited with excess share: Based on the requested transmission windows, the CMs sharing a cable channel are segregated into a group of underloaded CMs and a group of overloaded CMs [82], [83]. A CM is considered to be underloaded if the reported queue size (requested transmission window) is less than or equal to a prescribed maximum grant size divided by the number of CMs. An overloaded CM requested a transmission window larger than the maximum grant size. In the excess share mechanism, the total excess bandwidth is the sum of the remaining (unused) bandwidth of all underloaded CMs, which is then shared by the overloaded CMs. The grant for an overloaded CM becomes the maximum grant size plus the total excess bandwidth divided by the number of overloaded CMs.

3) Grant Scheduling Policy: The grant scheduling policy determines how multiple CM transmission windows (minislots) are arranged during a granting cycle. We employ the Shortest Propagation Delay First (SPD) scheduling policy [84] which arranges the CM grants in ascending order of their round-trip propagation delay from the MAC module. In particular, we follow a hybrid allocation of minislot resources [85] across the frequency and time dimensions such that the earliest available (in the time dimension) minislots are allocated in a greedy manner to the CMs with the shortest round-trip propagation delays.

B. UEPI Pseudowire (PW) Overhead Evaluation

The R-PHY architecture incurs overhead for two reasons: *i*) UEPI protocol on CIN, as well as *ii*) UEPI transport of REQ and maintenance frames. In contrast to the R-PHY architecture, the R-MACPHY architecture implements the DOCSIS MAC at the remote node. Thus, the R-MACPHY architecture does not need additional CIN transport mechanisms through UEPI interfaces and PWs. Therefore, the R-MACPHY does not experience the PW overheads for transporting the data information blocks from the remote node to the headend for the upper layer processing. In the remainder of this section, we evaluate the UEPI PW overhead incurred in the R-PHY architecture.

The RPD receives the upstream analog RF transmissions from the CMs in terms of DOCSIS frames over the cable link. These DOCSIS frames are processed to extract the REQ message and data payload. The UEPI protocol establishes multiple PWs for the transport of DOCSIS frame information to the headend (vMAC) with different priorities. The UEPI protocol uses standard IEEE 802.3 based Ethernet as the underlying technology for the transport of the DOCSIS frames in the digital format to the headend. For each UEPI packet, the 802.3 Ethernet header is 22 bytes, the IPv4 header is 20 bytes, the L2TPv2 header is 4 bytes, the Packet Streaming Protocol (PSP) subheader is 4 bytes, and the CRC is 4 bytes, resulting in a total overhead of 54 bytes per Ethernet frame. Thus, the overhead factor $\mathcal{O}$ due to the UEPI protocol for each Ethernet frame can be evaluated as $\mathcal{O} = 54/\mathcal{E}$, where, $\mathcal{E}$ is the Ethernet frame size. Although CableLabs specifications define the UEPI protocol, the actual framing of UEPI packets is implementation specific.

A given DOCSIS frame is typically mapped to several UEPI packets, separating payload data and REQ information for prioritization. Additionally, payload data and REQ information are mapped to UEPI packets based on the criteria of minimum and maximum UEPI Ethernet frame sizes. That is, large information blocks, such as payload data may be fragmented, and short information blocks, such as REQs, may be opportunistically aggregated across several SGs to conform with the prescribed minimum and maximum Ethernet frame sizes. Therefore, an accurate estimation of the overhead requires detailed knowledge of the distribution of the Ethernet frame sizes $\mathcal{E}$ and the resulting UEPI packet sizes. For UEPI packets based on the maximum Ethernet frame size $\mathcal{E}_{\max} = 1900$ bytes [68], the overhead factor is $\mathcal{O}^{\text{UEPI}}_{\min} = 54/1900 = 0.02842$, i.e., the overhead is 2.8 % of the UEPI frame. Note that this is the overhead due to the UEPI interface, which is specific to R-PHY. For smaller Ethernet frame sizes $\mathcal{E}$ and correspondingly smaller UEPI packets, the overhead $\mathcal{O}^{\text{UEPI}}$ increases proportionally. For instance, for $\mathcal{E} = 950$ bytes, the overhead is $\mathcal{O}^{\text{UEPI}} = 5.7$ %, while for $\mathcal{E} = 425$ bytes, the overhead due to UEPI climbs to $\mathcal{O}^{\text{UEPI}} = 11.4$ %. Note that this overhead due to UEPI affects only the transmission over the CIN, which has typically abundant transmission bit rate R_i, compared to the transmission bit rate of the cable network R_c. Therefore, the overhead due to UEPI is negligible when the cable network is the bottleneck.

In terms of the overhead due to DOCSIS REQ and maintenance frames over the CIN link, an entire UEPI packet carrying a single (or multiple) REQ(s) and maintenance frames can be considered as an overhead on a given CIN link. However, evaluating how many UEPI packets would carry REQ and maintenance frames within a given time duration is complex. The complexity arises from the required estimation of the UEPI packet size distribution. In an actual deployment, the UEPI interface implementation decides the UEPI packet size distribution. We model the number of UEPI packets with the variables $P^{\text{UPEI}}_{\text{data}}$ and $P^{\text{UPEI}}_{\text{non-data}}$ denoting the number of UEPI packets required to carry the data, as well as the request and maintenance information blocks within one t_{MAP} duration, respectively. The total number of UEPI packets P^{UPEI} required to transport the DOCSIS PHY frames to the vMAC at the headend within a single t_{MAP} duration is, $P^{\text{UPEI}} = P^{\text{UPEI}}_{\text{data}} + P^{\text{UPEI}}_{\text{non-data}}$. With $\mathcal{E}^{\text{non-data}}_{\text{avg}}$ and $\mathcal{E}_{\text{avg}}$ denoting the average frame sizes of the non-data UEPI packets and all UEPI packets (i.e., inclusive of data and non-data packets), respectively, the overhead $\mathcal{O}^{\text{RM}}$ from the REQ and maintenance UEPI packets on the CIN link, for a single t_{MAP} duration is

$$\mathcal{O}^{\text{RM}}_{\text{avg}} = \frac{P^{\text{UPEI}}_{\text{non-data}} \times \mathcal{E}^{\text{non-data}}_{\text{avg}}}{\left(P^{\text{UPEI}}_{\text{data}} + P^{\text{UPEI}}_{\text{non-data}}\right) \times \mathcal{E}_{\text{avg}}}. \tag{1}$$

The utilization impact of REQ and maintenance frames over the CIN link can be estimated as

$$\mathcal{U}^{\text{RM}}_{\text{avg}} = \frac{P^{\text{UPEI}}_{\text{non-data}} \times \mathcal{E}^{\text{non-data}}_{\text{avg}}}{R_i \times t_{\text{MAP}}}. \tag{2}$$

Suppose we conservatively consider the maximum UEPI Ethernet frame, i.e., 1900 bytes, the CIN data rate R_i = 1 Gbps, and one REQ frame corresponding to one SG in the duration of t_{MAP} = 2 ms. The resulting utilization $\mathcal{U}_{\text{RM}}$ of the CIN link for a single REQ and maintenance frame is $(1 \times 1900)/(1 \times 10^9 \times 0.002) = 9.5 \times 10^{-4}$, which is a very small fraction of the CIN link capacity R_i. Thus, the overheads due to conducting the DOCSIS MAC REQ and maintenance in the R-PHY architecture over the CIN are essentially negligible.

IV. DOCSIS Cable Polling Delay Analysis

This section presents a delay analysis of the DOCSIS polling protocol for upstream transmissions over the cable broadcast network. To the best of our knowledge, prior delay analyses of the DOCSIS protocol have mainly focused on the contention of bandwidth request (REQ) messages on the contention slots of the upstream MAC frames [30]–[36]. We consider piggybacking of the REQ messages on upstream data transmissions; thus, contention does not arise in our model (future work could combine prior contention models with our polling model). Polling protocols have been extensively analyzed for access networks based on passive optical networks (PONs), see [50]–[58].

A. Polling in R-PHY Architecture

In this section we present a basic timing analysis of the R-PHY bandwidth polling and upstream transmission dynamics. The goal of this timing analysis is to capture the main aspects of the DOCSIS protocol [59, Sec. 7.2] that govern the upstream transmission delays. Specifically, our goal is to gain insights into the elementary polling dynamics in the R-PHY architecture. For tractability, we focus on a single CM that is attached via a single RPD to a headend. We consider the Gated bandwidth allocation (grant sizing), which grants the CM its full request. Figure 8 illustrates the cyclical polling protocol exchanges between the considered CM and the DOCSIS MAC implemented at the headend (or cloud in the vMAC variant). The model notations are summarized in Table II. In a given cycle, the headend sends a MAP message that is forwarded by the RPD to the attached CM. As illustrated in Figure 8, the CM send its requests via the RPD to the headend/cloud, where the DOCSIS bandwidth allocation decisions are made. The corresponding grant is sent in a MAP message from the headend/cloud via the RPD to the CM. The CM in turn transmits its upstream data as instructed and piggybacks its next bandwidth request.

TABLE II
Model Parameters, With Default Settings

	Network Structure
R_c	Cable upstream transmission bit rate [bit/s] (CM to Remote Node (RN)) = 1 Gbps
R_i	CIN upstream transmission bit rate [bit/s] (RN to headend/cloud) = 10 Gbps
M	Number of CMs at considered RN
δ	One-way propagation delay from a CM to RN [s]
τ	One-way propagation delay between headend/cloud and RN [s]
$t^{\text{R-PHY}}_{\text{Mp}}$	$= \delta + \tau + t_{\text{MAP}}/2$; Mean MAP and prop. delay for one-way R-PHY network polling traversal, see Eq. (3)
$t^{\text{R-MAC}}_{\text{Mp}}$	$= \delta + t_{\text{MAP}}/2$; Mean MAP and prop. delay for one-way R-MACPHY network polling traversal
	Traffic Model
λ_c	Total packet generation rate [packets/s] of the M CMs at considered RN
λ_i	Base packet generation rate [packets/s] for CIN
$\bar{L}$	Mean packet size [bit]
σ^2_L	Variance of packet size [bit^2]
ρ_c	$= \bar{L}\lambda_c/R_c$ Relative cable traffic load (intensity) [unitfree]
ρ_i	$= \bar{L}\lambda_i/R_i$ Relative CIN base traffic load (intensity) of CIN [unitfree]
	Polling Protocol
t_{MAP}	Duration of bandwidth allocation MAP = 2 ms
G_n	Size of upstream transmission window [bit] granted to considered CM (or group of CMs) in cycle n
Z	Polling cycle duration [s]

1) One-Way R-PHY Network Traversal Delay: As ground work towards modeling the upstream packet delay, we first model the round-trip propagation delay of the R-PHY network as twice the one-way R-PHY network traversal delay $t^{\text{R-PHY}}_{\text{Mp}}$. In particular, we define for convenience (to reduce clutter) $t^{\text{R-PHY}}_{\text{Mp}}$ as the constant delay components due to physical propagation over the cable and CIN network, plus half the MAP period t_{MAP}. We consider half the t_{MAP} to model that a given arbitrary data packet may be generated at any (uniformly distributed) time instant during the MAP period. Thus, the packet experiences on average half the MAP period as delay from packet generation to next reporting. We apply similar reasoning for the grant transmission from headend to CM and then the actual CM data transmission. That is, we model

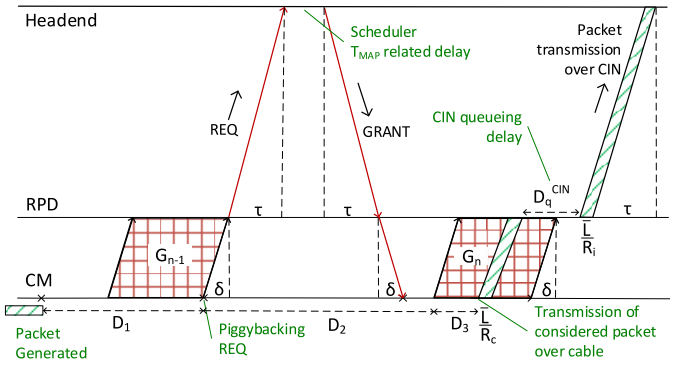

Fig. 8. Illustration of polling cycle timing for a cable modem (CM) in R-PHY architecture. A generated packet is reported via a request that is piggybacked on the CM upstream payload data transmission and forwarded by the remote PHY device (RPD) via the prioritized UEPI pseudowire (PW) for request (control) traffic to the headend. The headend allocates bandwidth and communicates the allocation via the MAP/grant DEPI to the RPD and onwards to the CM. According to the scheduled bandwidth allocation in the MAP, the CM sends its payload data, including the considered packet, upstream to the RPD. The RPD sends the data via the upstream data UEPI over the CIN to the headend.

that the propagation delays across the CIN and cable network are not specifically synchronized to the MAP periods, which appears realistic for real deployments with varying propagation delays. Thus, we include half the t_{MAP} for each transmission in a given direction over the network, resulting in the mean one-way R-PHY network traversal delay

$$t_{\text{Mp}}^{\text{R-PHY}} = \delta + \tau + \frac{t_{\text{MAP}}}{2}. \tag{3}$$

We neglect the overhead due to the transmission delay of the request message over the cable and the CIN network in this analysis (but consider the request message transmission delays in the simulations in Section V). Also, we assume that the request UEPI has negligible queueing delay in the RPD. Moreover, we neglect the schedule computation delay in the headend. For a refined analysis these neglected delay components could be included in a refined model for the network traversal delay $t_{\text{Mp}}^{\text{R-PHY}}$.

2) Polling Cycle Duration: The polling cycle corresponds to the round-trip propagation delay from the CM to the headend and back to the CM for the request and grant as well as the transmission time for the accumulated generated traffic over the cable link to the RPD, i.e., transmission time G_n/R_c for an accumulated data amount G_n. With the modeling of the one-way R-PHY network traversal delay in Eqn. (3), the mean cycle duration $E[Z]$ follows from [51, Eq. (7)]:

$$E[Z] = \frac{2t_{\text{Mp}}^{\text{R-PHY}}}{1-\rho_c}. \tag{4}$$

Note that the mean cycle duration is governed by the load (traffic intensity) on the cable network and is independent of the load on the CIN network. This is because the request and grant messages are transmitted with priority over the respective UEPI and DEPI CIN PW links. If these PWs achieve negligible transmission and queueing delays for the request and grant control messages over the CIN (relative to the round-trip propagation delay $t_{\text{Mp}}^{\text{R-PHY}}$ and the cable upstream data transmission delay G_n/R_c), then the CIN load has no significant effect on the cycle duration.

3) Upstream Packet Delay Components: We adapt the general polling protocol analysis from [51] to the R-PHY polling as illustrated in Figure 8. Following [51], we define the delay from the instant of packet generation to the piggybacked reporting at the end of the next upstream transmission as D_1. This delay D_1 corresponds to the residual life time of the polling cycle. According to general residual life time analysis [86, p. 173], the mean residual life time is

$$E[Z] = \frac{E[Z^2]}{2E[Z]}. \tag{5}$$

Applying Eqn. (5) to our setting by re-tracing the steps leading to [51, Eq. (35)] gives the mean of delay component D_1 as:

$$E[D_1] = \frac{t_{\text{Mp}}^{\text{R-PHY}}}{1-\rho_c} + \frac{\rho_c}{2R_c(1-\rho_c^2)}\left(\frac{\sigma_L^2}{\bar{L}} + \bar{L}\right). \tag{6}$$

We define the delay component D_2 as the time period between the CM report transmission and the beginning of the corresponding upstream data transmission. The delay component D_2 models the mean round-trip propagation delays (including the MAP delays) for the request from CM to the headend and the corresponding grant (MAP) from the headend to the CM. Accordingly,

$$E[D_2] = 2t_{\text{Mp}}^{\text{R-PHY}}. \tag{7}$$

The delay component D_3 models the time period from the starting instant of the cable upstream data transmission that contains the considered packet to the starting instant of the transmission of the considered packet. This D_3 delay corresponds to the transmission delay of the packets that were generated for the upstream transmission in cycle n before our considered packet. This time period of packet generation for cycle n before our packet corresponds to the backward recurrence time of a cycle. This backward recurrence time and the mean residual lifetime are equivalent for the considered steady state operation [87, Ch. 5.5]. That is, this packet generation time period has mean duration $E[Z^2]/(2E[Z])$, see Eqn. (5), during which packets are generated at rate λ. Each of the generated packets requires a mean transmission time of $\bar{L}/R_c$ over the cable link. Thus, the mean of delay component D_3 is

$$E[D_3] = \frac{\lambda \bar{L} E[Z^2]}{2R_c E[Z]} = \rho_c E[D_1]. \tag{8}$$

In addition to the delay components D_1, D_2, and D_3, the considered packet incurs the upstream transmission delay over the cable $\bar{L}/R_c$, the queueing delay D_q^{CIN} for the CIN transmission, the transmission delay over the CIN $\bar{L}/R_i$, and the one-way propagation delay $t_{\text{Mp}}^{\text{R-PHY}}$. Modeling the CIN queue with an M/G/1 model, we obtain for the mean waiting time in the CIN queue:

$$E\left[D_q^{\text{CIN}}\right] = \frac{\rho_i\left(\frac{\sigma_L^2}{\bar{L}} + \bar{L}\right)}{2R_i(1-\rho_i)}. \tag{9}$$

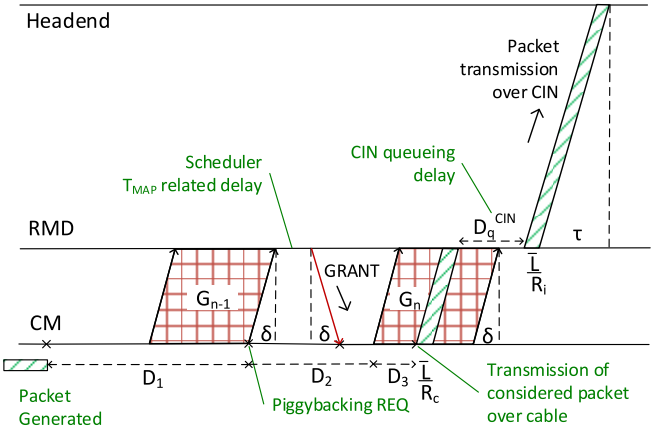

Fig. 9. Illustration of polling cycle timing for R-MAC architecture: The piggybacked CM request reaches the remote R-MACPHY (RMD) node via the cable link. The RMD processes the request and grants the bandwidth allocation to the CM. After the corresponding data packet transmission has reached the RMD, the packet is queued for CIN upstream transmission, and then transmitted from the RMD to the headend.

Combining all delay components, we obtain for the overall mean packet delay:

$$E[D] = 2t_{\mathrm{Mp}}^{\mathrm{R-PHY}}\frac{2-\rho_c}{1-\rho_c} + \bar{L}\left(\frac{1}{R_c}+\frac{1}{R_i}\right) + \frac{1}{2}\left(\frac{\sigma_L^2}{\bar{L}}+\bar{L}\right)\left(\frac{\rho_c}{R_c(1-\rho_c)}+\frac{\rho_i}{R_i(1-\rho_i)}\right). \quad (10)$$

B. R-MACPHY Timing Analysis

The R-MACPHY polling cycle includes only the propagation delay of the cable link δ, as illustrated in Figure 9. The potentially long propagation delay τ from the remote node to the headend does not arise for the R-MACPHY polling. Thus, we set the one-way propagation delay for the R-MACPHY polling analysis to $t_{\mathrm{Mp}}^{\mathrm{R-MAC}} = \delta + t_{\mathrm{MAP}}/2$. The R-MACPHY polling dynamics are essentially the same as for the R-PHY architecture and we can re-trace the R-PHY delay analysis with the shorter $t_{\mathrm{Mp}}^{\mathrm{R-MAC}}$ to obtain the mean packet delay for R-MACPHY. However, this re-traced analysis does not include the one-way CIN propagation delay τ. Thus, the total mean delay for R-MACPHY is the delay expression (10), evaluated with $t_{\mathrm{Mp}}^{\mathrm{R-MAC}} = \delta + t_{\mathrm{MAP}}/2$ plus the one-way CIN propagation delay τ.

C. R-PHY vs. R-MACPHY Analysis Comparison

For low traffic loads $\rho_c \to 0$, $\rho_i \to 0$, the mean R-PHY packet delay (10) approaches

$$\lim_{\rho_c\to 0,\rho_i\to 0} E\left[D^{\mathrm{R-PHY}}\right] = 4\left(\delta+\tau+\frac{t_{\mathrm{MAP}}}{2}\right)+\frac{\bar{L}}{R_c}+\frac{\bar{L}}{R_i}. \quad (11)$$

In contrast, the mean R-MACPHY packet delay approaches

$$\lim_{\rho_c\to 0,\ \rho_i\to 0} E\left[D^{\mathrm{R-MAC}}\right] = 4\left(\delta+\frac{t_{\mathrm{MAP}}}{2}\right)+\tau+\frac{\bar{L}}{R_c}+\frac{\bar{L}}{R_i}. \quad (12)$$

Thus, R-MACPHY reduces the mean packet delay at low loads by 3τ compared to R-PHY. Recall that the parameter τ represents the one-way CIN propagation delay. Thus, for a given CIN infrastructure, the parameter is constant. However, when comparing different CIN options, the parameter τ is variable. The range of the parameter τ corresponds directly to the CIN one-way propagation distance. Additional delays may be incurred on the CIN due to queueing and store-and-forward in intermediate switches.

Although we focus on upstream data packet transmission in this study, we briefly note that both R-PHY and R-MACPHY have essentially equivalent downstream packet delays. The downstream delay is mainly composed of the CIN queueing delay, which can be modeled analogous to Eqn. (9), the packet transmission delays over the CIN and cable networks, plus the one-way network traversal delay t_{Mp} (3).

V. Numerical Performance Comparison

A. Simulation Setup

1) Overview: We developed a simulation model of the link layer DOCSIS protocol operating in the R-PHY and R-MACPHY architectures using the discrete event simulator OMNET++. We simulate the broadcast cable based access network illustrated in Fig. 1 for a single remote node serving one SG of multiple CMs. The digital Ethernet CIN network between the simulated remote node and the headend is loaded by the traffic from the simulated remote node as well as a CIN base traffic load ρ_i. The CIN base traffic load ρ_i could originate from other remote nodes (servicing other SGs) or from other access networks. We focus on simulating one remote node with its attached CMs in detail in order to gain insights into the polling dynamics with a remote node operating as either a Remote PHY node (RPD, see Fig. 3) or a Remote MACPHY node (RMD, see Fig. 6).

Although DOCSIS 3.1 can support different QoS levels for different applications [88], we focus on best-effort service [89] in this first comparative evaluation of the R-PHY and R-MACPHY architectures. Moreover, we focus on the DOCSIS data services and do not consider EQAM video services.

2) Cable Network: For typical broadcast cable deployment scenarios, the average number of HouseHolds Passed (HHP) for a given remote node can be up to 450 CMs, which may belong to several SGs. A typical average number of CMs connected to a remote node is around 200 CMs [90]. A given set of physical resources are commonly shared among all the CMs in a given SG. The resource allocation to each individual CM in a given SG is controlled by the scheduler (see Section III-A). Under high utilization scenarios the number of CMs per SG can reach up to 400 CMs [91]. Therefore, we consider SG sizes M ranging from 200 to 400 CMs in our simulations.

The recent DOCSIS 3.1 version supports both upstream and downstream data peak throughputs on the order of Gbps [92]. DOCSIS 3.1 includes Orthogonal Frequency Division Multiplexing (OFDM) for the physical layer modulation over the broadband spectrum to achieve high spectral

efficiency [93]–[95]. DOCSIS 3.1 also incorporates high levels of QAM modulation (up to 16K), Low Density Parity Check (LDPC) Forward Error Correction (FEC), and a wide spectrum of 1.2 GHz in the downstream and 204 MHz in the upstream [93]. We set the transmission bit rate of the cable uplink channel to $R_c = 1$ Gbps. The upstream transmissions from all CMs attached to the remote node share the upstream cable transmission bit rate R_c.

The distance from the CMs to the remote node, i.e., the RPD or RMD, can be estimated based on the number of Actives (RF amplifiers) in the cable link. Typically, a single coaxial broadcast cable segment can run up to a distance of 600–900 feet. Additionally, there can be a cascade depth of 4 to 5 Actives from a remote node to the CMs. Five Actives support five coaxial segments reaching up to the distance of, say, $5 \times 600 = 3000$ feet in total. We consider the CM-to-remote node one-way distance to be uniformly distributed between 1 and 2 km in our simulations and set the one-way cable propagation delay δ accordingly.

Throughout, we assume that 20 % of the cable transmission bit rate R_c is occupied with contention and maintenance slots. Thus, only 80 % of the cable transmission bit rate R_c are available for data transmissions. In each cycle, each CM sends a request message of 64 bytes upstream in piggybacked manner to communicate its queue occupancy to the MAC module.

3) CIN Network: We vary the CIN distance from the remote node (RPD or RMD) to the headend from 10 to 2000 miles, considering that a WAN digital Ethernet link can span for long distances to cloud locations. In our simulations, we model the logical Ethernet CIN link over the CIN network as an infinite-sized queue that is drained by a link with transmission bit rate $R_i = 10$ Gbps and has one-way propagation delay τ leading to the headend.

4) Traffic Model: Following widely used traffic models for access networks, we consider self-similar traffic [96]. We vary the level of burstiness of the self-similar traffic from Hurst parameter value $H = 0.5$, corresponding to Poisson traffic, to $H = 0.925$, which corresponds to highly bursty traffic. Each CM independently generates self-similar data packet traffic, whereby the packet sizes are distributed as follows: 60 % 64 byte packets, 4 % 300 byte packets, 11 % 580 byte packets, and 25 % 1518 byte packets, i.e., the mean packet size is $\bar{L} = 494$ bytes. Initially, we assume that each CM has unlimited buffering, i.e., there are no losses and the long-run throughput is equal to the offered traffic load (for the considered stable network operating scenarios); finite CM buffers are considered in Section V-E. We vary the aggregate data packet generation rate λ_c of the CMs attached to the simulated remote node to achieve prescribed levels of cable network traffic (load) intensity $\rho_c = \lambda_c \bar{L}/R_c$ (see Table II). All CMs at the simulated remote node contribute equally to the aggregate packet generation rate λ_c.

We load the CIN network with a base traffic load $\rho_i = \lambda_i \bar{L}/R_i$ that we keep fixed at $\rho_i = 0.5$ for $R_i = 10$ Gbps throughout the evaluations presented in this section. This CIN base traffic has always the same Hurst parameter as the traffic in the cable network. Note that the total CIN traffic load is the base CIN load plus the traffic from the one simulated cable network, i.e., the total CIN traffic intensity is $(\lambda_c + \lambda_i)\bar{L}/R_i$.

5) Performance Metrics: We define the packet delay as the time period from the time instant of packet generation at a CM to the time instant of the complete packet delivery to the headend (CCAP core). The average of the packet delays sampled from over 300 s of simulated network operation forms the mean packet delay reported in Sections V-B–V-D. The packet loss rate considered in Section V-E is defined as the long-run ratio of the number of lost packets to the number of generated packets.

B. Offline Scheduling With Gated Bandwidth Allocation

Initially, we cross-validate the analytical delay model from Section IV with the simulation model. We consider offline scheduling with Gated bandwidth allocation, see Section III-A. A single CM generating Poisson traffic is attached to the considered RPD/RMD.

1) Single Cable Modem (CM) With Poisson Traffic: Fig. 10 shows the mean packet delay of the R-PHY and R-MACPHY networks as a function of the traffic intensity ρ_c on the cable upstream link. More specifically, Figs. 10(a), (b), and (c) consider relatively short one-way CIN distances between the RPD/RMD and the headend of 12.5, 50, and 100 miles. The 50 miles distance corresponds to the CM-to-CMTS distance for conventional (non-modular) DOCSIS 3.1 networks [59], while DOCSIS 3.0 has a limit of 100 miles [97]. The longer distances of 500, 1000, and 2000 miles, which arise with cloud vMAC operation, see Section II-B3a, are considered in Figs. 10(d), (e), and (f). We observe from Fig. 10(a) that the analytical model has relatively large deviations from the simulations for the very short CIN distance of 12.5 miles. These discrepancies appear to be due to our assumption that each traversal across the network incurs the t_{Mp} delay due to physical propagation and the waiting time until the next MAP period (whereby the MAP period is denoted by t_{MAP}), see Section IV and in particular Eqn. (3).

In order to examine the impact of this assumption we have varied the factor associated with t_{Mp} in Eqn. (10) as well as the divisor of t_{MAP} in Eqn. (3). We found that alternate factors/divisors may lead to a closer match between analysis and simulation. Specifically, we found that the combinations of factor 3 and divisor 2 for R-PHY, as well as factor 3 and divisor 4 for R-MACPHY, which are plotted as "alt." in Fig. 10 give relatively close matches for the short CIN scenarios. The improvement in accuracy with these alternate factors/divisors is likely due to a particular alignment of the MAP period boundaries with the typical arrival and dispatch times of control messages. That is, these alignments are possibly not uniformly random, but follow some different distribution. Future research could further explore the underlying reasons for these modeling discrepancies in more detail. However, we note that the discrepancies have relatively small magnitude and are visible only for short CIN scenarios. Importantly, we observe from Fig. 10(c) for the longer 100 miles CIN distance and particularly from Figs. 10(d), (e), and (f) for the

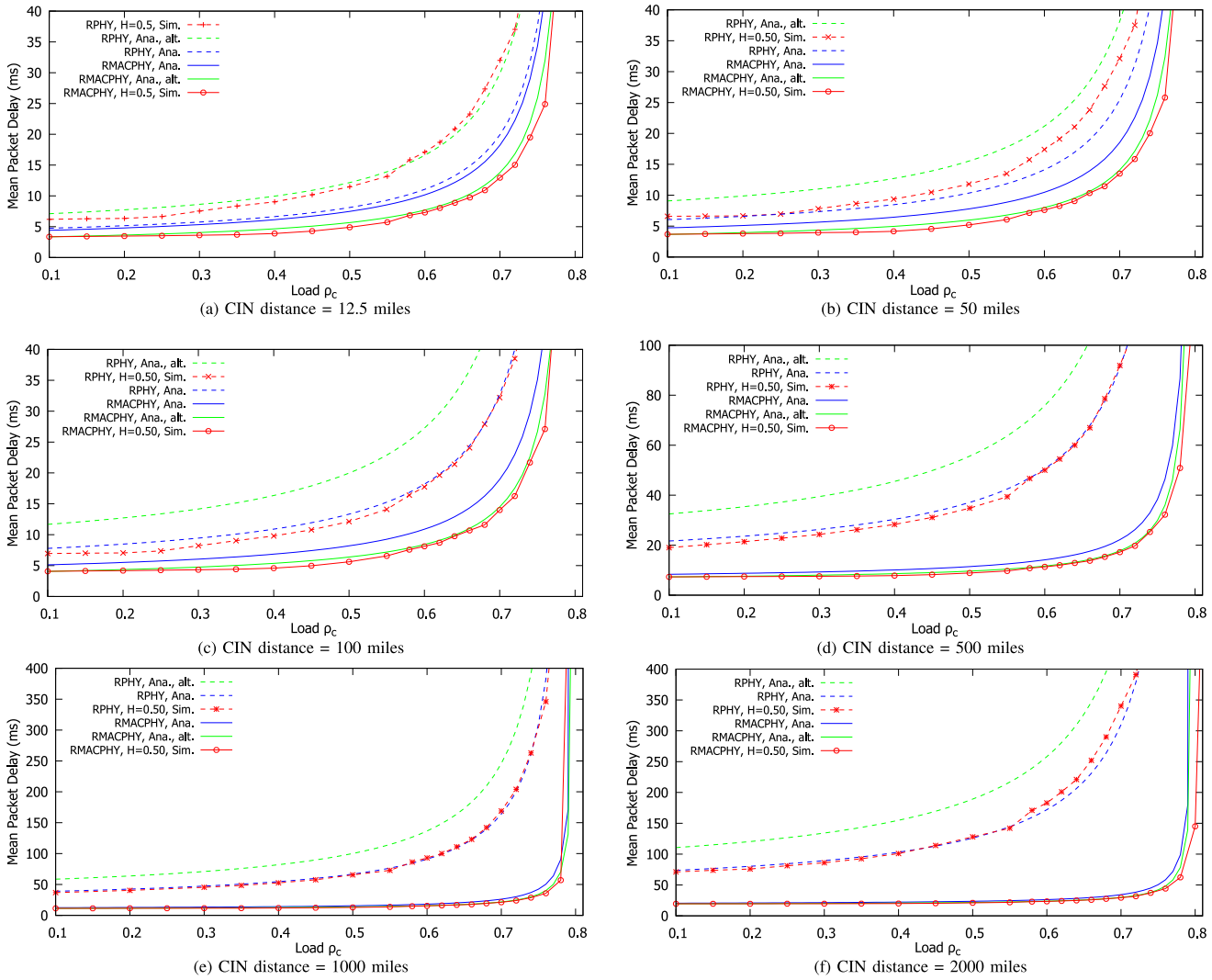

(a) CIN distance = 12.5 miles
(b) CIN distance = 50 miles
(c) CIN distance = 100 miles
(d) CIN distance = 500 miles
(e) CIN distance = 1000 miles
(f) CIN distance = 2000 miles

Fig. 10. R-PHY vs. R-MACPHY mean packet delay as a function of cable link traffic intensity ρ_c for CIN one-way distances ranging from 12.5 to 2000 miles; fixed parameters: CIN base traffic intensity $\rho_i = 0.5$, one CM, gated bandwidth allocation, 20 % of cable capacity for contention and maintenance.

distances above 100 miles that the analytical and simulation models achieve relatively close correspondence.

We observe from the initial evaluation results in Figs. 10(c)–(f) that R-MACPHY achieves significantly lower mean packet delays than R-PHY for long CIN distances and for moderate to high traffic load levels ρ_c on the cable link. For instance, for a CIN distance of 500 miles and $\rho_c = 0.6$, R-PHY incurs over twice the delay of R-MACPHY. The lower mean packet delay with R-MACPHY is due to the "localized" MAC scheduling in the remote node (RMD), which avoids the long round-trip delay over the CIN for the request-grant signalling.

Throughout the evaluations in Fig. 10, contention and maintenance slots take up 20 % of the MAP. Thus, effectively only 80 % of the cable upstream transmission bit rate R_c is available for upstream data packet transmissions. We observe that R-PHY has generally pronounced delay increases well before approaching the effective upstream capacity (stability limit) of $0.8R_c$. In contrast, R-MACPHY continues to provide low delays for moderate to high loads that quite closely approach the stability limit. R-MACPHY then has sharply increasing delays very close to the stability limit. This R-MACPHY behavior is a positive feature: R-MACPHY consistently provides very low delays across the entire load range, up to very close to the stability limit. R-MACPHY gives substantial delay increases only when the system is loaded very close to the stability limit.

2) Multiple Cable Modems (CMs) With Self-Similar Traffic: We proceed to compare the performance of R-PHY and R-MACPHY for different numbers of CMs attached to a given remote node and for different levels of traffic burstiness in Fig. 11. Figs. 11(a) and (b) show the mean upstream packet delay as a function of the traffic intensity on the cable upstream channel ρ_c for different levels of traffic burstiness for a fixed number of $M = 200$ CMs that are attached to the considered remote node. We consider a CIN distance of 50 miles as representative for the R-PHY variant with MAC processing in the headend (see Section II-B3a) and the CIN distance of 500 miles ($\tau = 4.05$ ms) as representative of cloud vMAC processing (see Section II-B3b). We increase the traffic burstiness by increasing the Hurst parameter H of the self-similar traffic. We observe from Figs. 11(a) and (b)

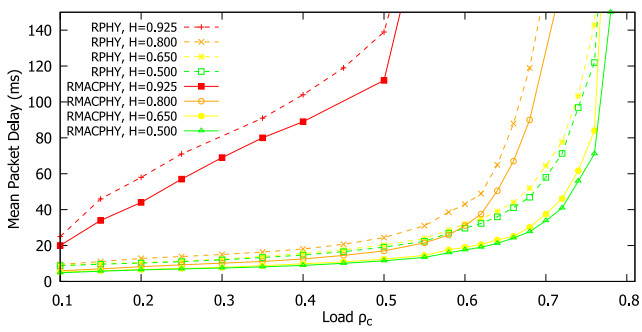

(a) Different Hurst parameters for CIN dist. = 50 miles, $M = 200$ CMs

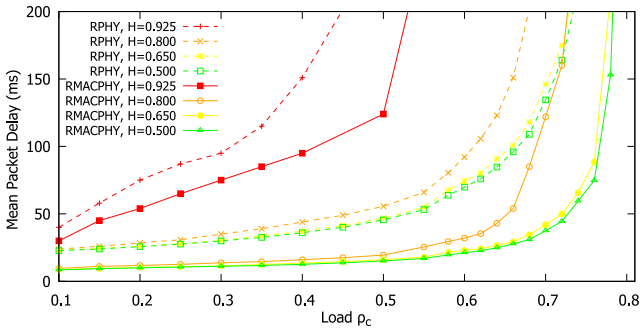

(b) Different Hurst parameters for CIN dist. = 500 miles, $M = 200$ CMs

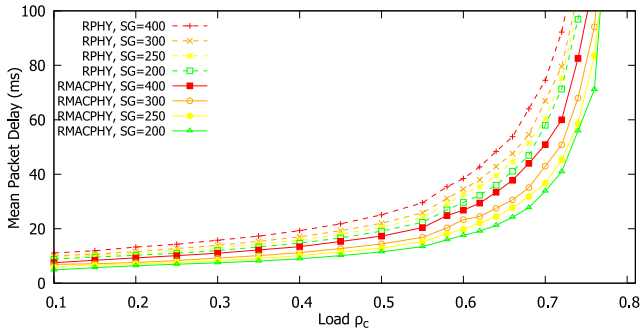

(c) Different SG sizes M for CIN distance = 50 miles, $H = 0.5$ traffic

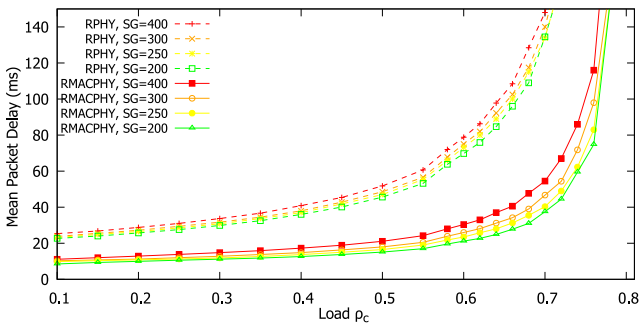

(d) Different SG sizes M for CIN distance = 500 miles, $H = 0.5$ traffic

Fig. 11. R-PHY vs. R-MACPHY mean packet delay as a function of cable link traffic intensity ρ_c for different levels of traffic burstiness (i.e., different Hurst parameters) and different numbers of CMs in a service group attached to a given remote node for different CIN one-way distances; fixed parameters: CIN base traffic intensity $\rho_i = 0.5$, gated bandwidth allocation, 20 % of cable capacity for contention and maintenance.

that the delay differences between R-PHY and R-MACPHY follow the same general pattern as for Poisson traffic in Fig. 10. However, pronounced delay differences occur at lower loads. For instance, for Poisson traffic, we observed very pronounced higher R-PHY delay compared to R-MACPHY at load $\rho_c = 0.7$, see Figs. 10(b) and (d). For bursty self-similar traffic, the delay differences become very pronounced at lower loads, e.g., $\rho_c = 0.6$, especially for the long 500 miles CIN distance, see Fig. 11(b) (in comparison to the corresponding Fig. 10(d)).

We also observe from Figs. 11(a) and (b) that the effects of the traffic burstiness are especially pronounced for the highly bursty traffic with $H = 0.925$. For $H = 0.925$, we observe significant delay differences between R-PHY and R-MACPHY of around 10 ms already for low loads above $\rho_c = 0.15$. For a CIN distance of 500 miles, for instance, R-PHY achieves mean delays below 100 ms only for loads up to around $\rho_c = 0.3$, whereas R-MACPHY achieves delays below 100 ms for loads up to around $\rho_c = 0.4$ for this highly challenging $H = 0.925$ traffic. These pronounced effects of high levels of burstiness are in agreement with earlier studies in access networks, e.g., [98]. We conclude that for the highly bursty $H = 0.925$ traffic, the faster dynamic bandwidth allocation in the remote RMD node in the R-MACPHY architecture can significantly reduce the mean packet delay already for low network loads. In contrast, for traffic with lower levels of burstiness in the short 50 miles CIN setting (see Fig. 11(a)), R-PHY and R-MACPHY give very similar mean packet delays up to moderate load levels.

Figs. 11(c) and (d) evaluate the mean packet delay for R-PHY and R-MACPHY nodes with respect to the number M of CMs connected to the remote node for Poisson (i.e., $H = 0.5$) traffic. We observe from Figs. 11(c) and (d) that increasing numbers M of CMs slightly increase the mean packet delays. The delay increases are most pronounced in the moderately high load range for ρ_c ranging from 0.6 to 0.75 and are very similar for both R-PHY and R-MACPHY. The delay increases with increasing CM numbers are due to the overhead for the request messages. In our simulations, each CM sends a 64 byte request message in each cycle (piggybacked onto upstream data transmission, or separately if CM has no data to send). With M denoting the number of CMs and Z denoting the cycle duration, these request message increase the relative cable channel load by

$$\text{Request Message Overhead} = \frac{64 \times 8 \times M}{0.8 \times R_c \times Z}. \qquad (13)$$

The resulting delay increases are most pronounced in the moderately high load range where (*i*) the cycle durations Z are still short enough so that the request messages cause a noticeable additional load, and (*ii*) the cable channel has high enough load ρ_c from the payload traffic that the additional load from the request messages results in noticeable delay increases. As the traffic load approaches the $0.8R_c$ available cable channel transmission bit rate, the cycle duration Z of the Gated allocation considered in Figs. 11(c) and (d) grows very long, resulting in a negligible load increase due to the request messages.

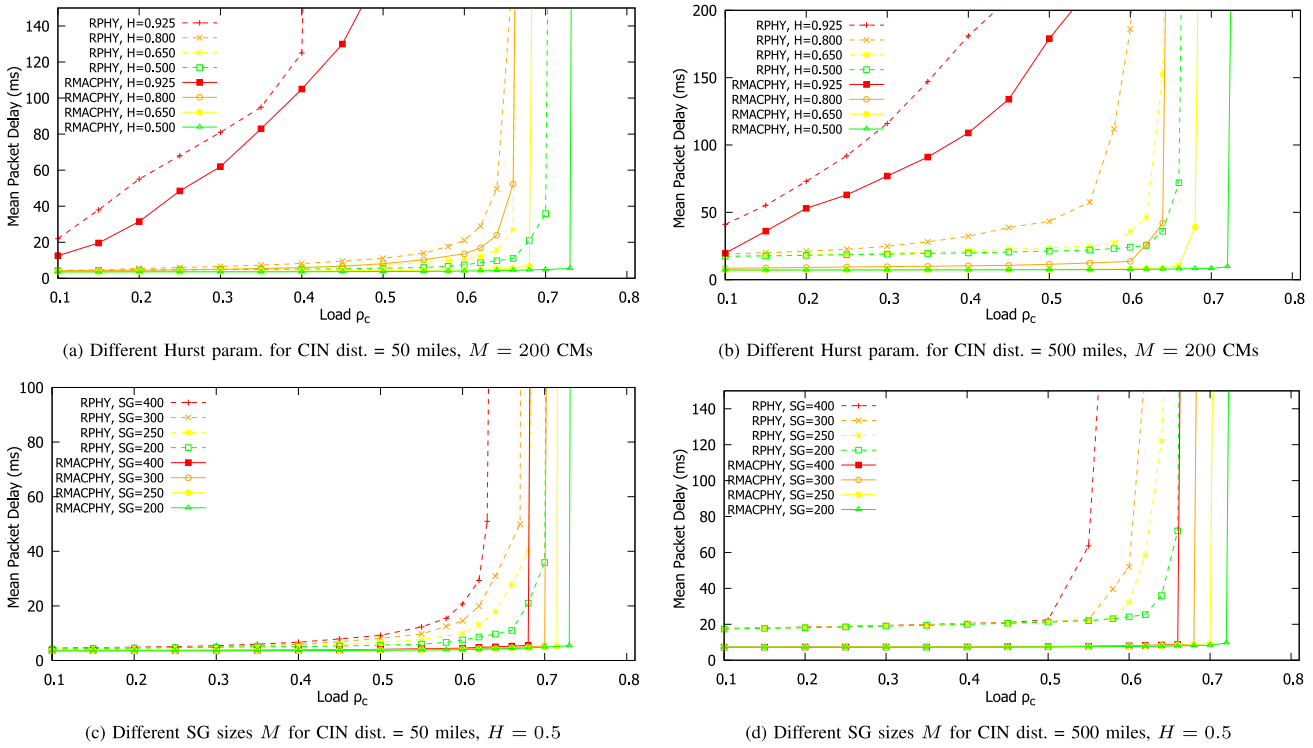

(a) Different Hurst param. for CIN dist. = 50 miles, $M = 200$ CMs

(b) Different Hurst param. for CIN dist. = 500 miles, $M = 200$ CMs

(c) Different SG sizes M for CIN dist. = 50 miles, $H = 0.5$

(d) Different SG sizes M for CIN dist. = 500 miles, $H = 0.5$

Fig. 12. R-PHY vs. R-MACPHY mean packet delay for double-phase polling (DPP) with excess share grant sizing as a function of cable link traffic intensity ρ_c for different levels of traffic burstiness and different number of CMs attached to a given remote node, for different CIN one-way distances; fixed parameters: CIN base traffic intensity $\rho_i = 0.5$, 20 % of cable capacity for contention and maintenance.

C. Double-Phase Polling (DPP) With Excess Share Bandwidth Allocation

In this section we compare the performance of R-PHY and R-MACPHY for double-phase polling (DPP) with excess bandwidth sharing [78], [99]. The simulation evaluations for DPP with excess bandwidth sharing are motivated as follows. DOCSIS protocol versions 3.0 and 3.1 permit multi-thread scheduling (or pipelined scheduling) [46] using multiple outstanding requests as described in [59, Sec. 7]. A CM may have multiple outstanding requests, i.e., the CM can send additional requests without having received a grant or grant-pending in the form of an acknowledgment for an earlier request.

Multi-thread (pipelined) scheduling is generally well suited to mask the long propagation delays in polling MAC systems covering long distances [100], [101]. However, multi-thread polling is also quite complex and requires complex thread tuning [102]. A recent study [103] has demonstrated that the simple double phase polling scheduling with excess bandwidth sharing DBA [78], [99] gives essentially equivalent performance to the complex multi-thread polling in long-propagation delay polling systems.

A critical aspect of polling-based MAC is masking the idle times that may arise due to the long propagation delays between the CM transmission of a request message and the arrival of the corresponding grant message to the CM. In the DPP mechanism, the polling cycle of one CM group is interleaved with the transmissions of the other CM group so as to mask the idle times between request and transmission. In order to enable this masking, we set the maximum aggregate grant size $G_{\max}$ [bit] for a DPP group to mask the round-trip propagation delay between the CMs and the scheduler. In particular, we set $G_{\max}$ such that the transmission time of the maximum grant size $G_{\max}$ upstream over the cable link (with $0.8R_c$ available transmission bit rate for data) corresponds to the smallest integer multiple of the MAP duration t_{MAP} that exceeds the mean round-trip propagation (network traversal) delay $2t_{\text{Mp}}$, i.e.,

$$G_{\max} = 0.8R_c \left\lceil \frac{2t_{\text{Mp}}}{t_{\text{MAP}}} \right\rceil t_{\text{MAP}}. \tag{14}$$

Thus, when one DPP polling group has enough data traffic to utilize the maximum permitted grant size $G_{\max}$, the upstream data transmission time $G_{\max}/(0.8R_c)$ of this DPP group will mask the round trip propagation delay for the requests and grants of the other DPP group. We note that in order to mask the worst case round-trip propagation (network traversal) delay $2(t_{\text{MAP}}+\delta+\tau)$, a correspondingly larger $G_{\max}$ setting would be needed. However, we found that the $2(t_{\text{MAP}}+\delta+\tau)$ worst-case delay occurs very rarely and the larger $G_{\max}$ would make DPP bandwidth allocation slightly less responsive; therefore, we consider the $G_{\max}$ setting based on the mean network traversal delay as per Eqn. (14).

Comparing Figs. 12(a) and (b) with Figs. 11(a) and (b), we observe that for the highly bursty $H = 0.925$ traffic, DPP gives about the same or slightly higher mean packet delays than Gated allocation; whereas for the lower traffic burstiness levels $H \leq 0.8$, DPP achieves significant mean delay reductions compared to Gated allocation. For the highly bursty $H = 0.925$ traffic, a single (or very few) CM(s) may have a very large traffic burst at a time, while all other CMs have

no traffic. If only CMs in one DPP polling group have data traffic, the other polling group cannot effectively mask the propagation delay. Rather, the limitation of the DPP cycle duration (to approx. $Z_{\mathrm{DPP}} = 2t_{\mathrm{Mp}} + G_{\max}/(0.8R_c)$) introduces frequent request messages that increase the overhead compared to Gated allocation, which requires only one request message for an arbitrarily large traffic burst (i.e., has no grant size limit).

For low to moderate traffic burstiness, e.g., for $H \leq 0.8$, the traffic burst are typically spread over CMs from both DPP polling groups. For such balanced loading of the two DPP polling groups, the upstream transmissions of one group can effectively mask the round-trip propagation delay for the request and grant messages of the other group, resulting in significant reductions of the mean packet delays compared to Gated allocation. This masking effect of DPP can effectively extend the operating range of R-PHY for low-delay applications, e.g., we observe from Fig. 12(b) that for load $\rho_c = 0.58$ of $H = 0.65$ traffic, R-PHY achieves a mean packet delay of 27.3 ms, whereas Gated gives a corresponding mean packet delay of 67.6 ms in Fig. 11(b). Importantly, we observe from Fig. 12(a) that for traffic with low to moderate levels of burstiness ($H \leq 0.8$) and cable traffic loads up to a moderately high level of $\rho_c = 0.6$ (which corresponds to $0.6/0.8 = 75$ % effective utilization of the available data upstream transmission bitrate), both R-PHY and R-MACPHY give very similar performance when DPP is employed up to the CIN distance of 50 miles. In particular, both R-PHY and R-MACPHY achieve mean packet delays below 20 ms for up to 75 % effective utilization of the available transmission bitrate (and delays below 10 ms for effective utilizations up to $0.5/0.8 = 62.5$ %; below 6 ms for up to $0.25/0.8 = 31$ % effective utilization).

Figs. 12(c) and (d) evaluate the effects of SG size M on the mean packet delay for the R-PHY and R-MACPHY architectures with DPP. Comparing the DPP mean packet delays in Figs. 12(c) and (d) with the corresponding Gated delays in Figs. 11(c) and (d), we observe that with Gated, the delays increase gradually with increasing load; whereas with DPP, the delays are essentially constant up to a "knee point" and then increase abruptly. This "knee point" behavior is particularly pronounced for R-MACPHY, which in Fig. 12(d) gives essentially constant 7.3 ms mean delay up to knee points located at approximately $\rho_c = 0.66$ for 400 CMs and roughly at $\rho_c = 0.72$ for 200 CMs. For the 500 Mile CIN distance, the DPP maximum grant size is set to $G_{\max} = 6t_{\mathrm{MAP}} \times 0.8R_c$ for R-PHY and $G_{\max} = t_{\mathrm{MAP}} \times 0.8R_c$ for R-MACPHY, according to Eqn. (14). Correspondingly, R-MACPHY has roughly a six times higher DPP request message frequency and overhead compared to R-PHY. The frequent request messages and "localized" bandwidth allocation in the remote RMD node make R-MACPHY with DPP highly responsive, ensuring low delay packet service up to data (plus request message) traffic loads very close to the $0.8R_c$ available cable upstream transmission bit rate. [The frequent request messages with R-MACPHY increase the overhead and result in higher packet loss rates than R-PHY for very high load levels (beyond the practically relevant load range), see Fig. 14 and Section V-E.] In contrast, the R-PHY architecture is less responsive due to the bandwidth allocation at the headend, leading to a more gradual delay increase than for R-MACPHY. Nevertheless, R-PHY with DPP achieves significant mean packet delay reductions compared to Gated allocation. For instance, for 500 miles CIN distance and $\rho_c = 0.5$ load, the mean packet delay of 48.6 ms for $M = 300$ CMs with Gated (Fig. 11(d)) is reduced to 21.6 ms with DPP (Fig. 12(d)). For the 50 miles CIN, we observe from Fig. 12(c) that R-PHY and R-MACPHY give very similar mean packet delays for all considered numbers of CMs up to a moderately high load of $\rho_c = 0.6$ (whereby the delays are below 6 ms for loads up to $\rho_c = 0.5$).

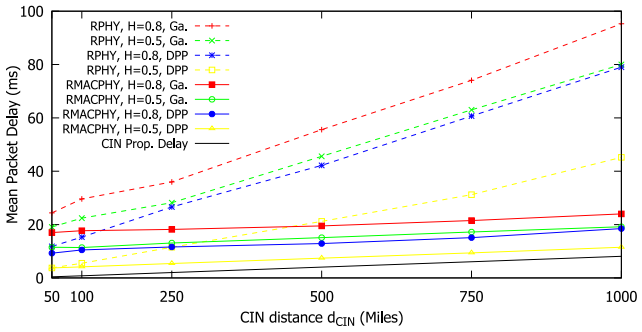

Fig. 13. R-PHY vs. R-MACPHY mean packet delay performance for Self-Similar ($H = 0.8$) and Poisson ($H = 0.5$) traffic as a function of CIN distance; fixed parameters: Cable link traffic intensity $\rho_c = 0.5$, CIN base traffic intensity $\rho_i = 0.5$, 200 CMs, 20 % of cable capacity for contention and maintenance.

D. Mean Delay as a Function of CIN Distance

In order to gain further insight into the impact of the CIN distance, which is a key parameter considered in the planning of R-PHY and R-MACPHY networks, we examine the mean packet delay as a function of CIN distance in Fig. 13. From Fig. 13 we observe that R-MACPHY achieves a very significant reduction of average packet delay as compared to R-PHY. As the maximum CIN propagation delay is increased, the performance differences between R-MACPHY and R-PHY become more pronounced. For the CIN distance of 1000 miles, the R-PHY mean packet delay is over four times higher than the R-MACPHY mean packet delay.

Examining the results for R-PHY and Poisson traffic ($H = 0.5$), in Fig. 13 more closely, we observe that DPP with excess bandwidth sharing achieves a substantially lower mean packet delays than Gated scheduling. For instance, when the CIN distance is 100 miles, the Gated scheduling yields an average mean packet delay of 22.4 ms, while DPP yields an average mean delay of 5.5 ms which is a 75 % decrease, illustrating the impact of the scheduling mechanism. In addition, the mean packet delay for DPP with excess bandwidth sharing for bursty traffic ($H = 0.8$) is lower than the delay for Gated scheduling of Poisson traffic.

We proceed to contrast our results to the results presented in Chapman *et al.* [46] who examined the impact of the CIN distance on the R-PHY architecture. Reference [46, Fig. 20] considers the REQ-GRANT scheduler, which closely follows the protocol of our Gated and DPP mechanisms, at 50% load (i.e., $\rho_i = 0.5$). Fig. 13 shows a linear increase in the mean packet delay with respect to CIN distances for both the R-PHY

and R-MACPHY architectures. For example, the mean packet delay varies linearly from 3.5 ms to 21.5 ms for Poisson traffic and DPP scheduling in the R-PHY architecture for CIN distances between 50 and 500 miles. In [46, Fig. 20] the corresponding mean packet delays roughly range from 5 ms to 20 ms which are comparable to our results. The near linear increase of the R-PHY DPP mean packet delay has significantly higher slope than the corresponding R-MACPHY DPP delay. Thus, R-PHY gives significantly higher delays than R-MACPHY for long CIN networks.

Importantly, we observe from Fig. 13 that self-similar traffic gives substantially higher slopes of the mean packet delay as a function of CIN distance than Poisson traffic. For instance, we observe that the mean packet delay for self-similar traffic with $H = 0.8$ increases near linearly to close to 80 ms for the 1000 miles CIN distance in R-PHY. In contrast, the slope for $H = 0.8$ for DPP is very low for R-MACPHY and the mean packet delay stays below 20 ms for a 1000 miles CIN distance. Thus, the mean packet delay of R-PHY is four times higher than the R-MACPHY mean packet delay for a 1000 miles CIN. One-way mean packet delays on the order of 80 ms may negatively impact the QoS of real-time packet traffic that has to traverse two access networks as well as a long-distance core network on the end-to-end path. Thus, R-MACPHY appears better suited to provide real-time QoS for access networks with long CIN distances.

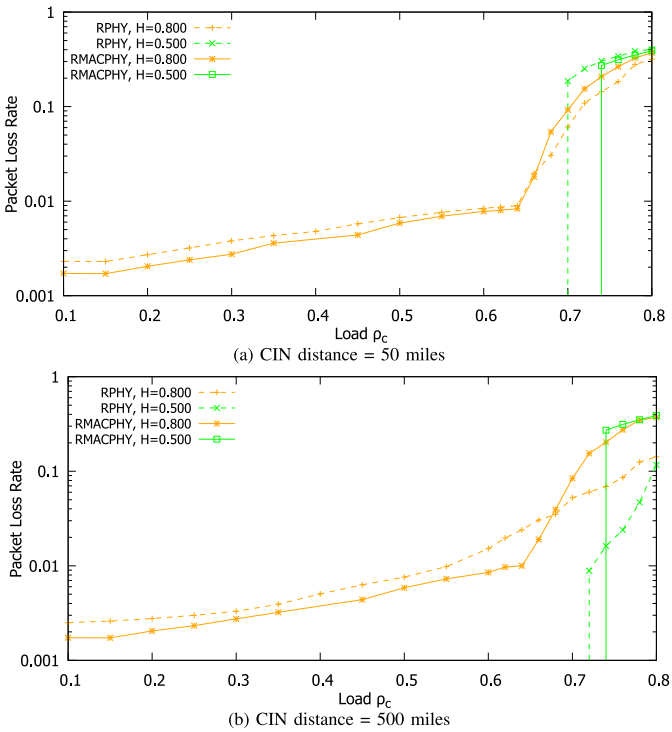

Fig. 14. R-PHY vs. R-MACPHY packet loss rate for double-phase polling (DPP) scheduling with excess share grant sizing, as a function of cable link traffic intensity ρ_c for different CIN one-way distances; fixed parameters: CM buffer size 12.5 kbyte, CIN base traffic intensity $\rho_i = 0.5$, 200 CMs, 20 % of cable capacity for contention and maintenance.

E. Packet Loss Rate

We compare the packet loss rates of the R-PHY and R-MACPHY architectures by simulating a limited buffer (with First-In-First-Out (FIFO) queuing and tail drop) in each CM. We considered typical CM buffer capacities, including 12.5 kbyte and 64 kbyte as considered in [88]. Due to space constraints, we present only plots for the 12.5 kbyte buffer capacity, which exhibits the typical packet loss dynamics, in Fig. 14. We observe from Fig. 14 that for both 50 and 500 miles CIN distance, the loss rates stay below 1 % for the moderately bursty ($H = 0.8$) traffic up to a cable traffic load of $\rho_c = 0.64$ (resp. below 3 % for R-PHY for 500 miles); additional evaluations found less then 1 % loss rate for up to $\rho_c = 0.66$ for 64 kbyte CM buffers. We also observe from Fig. 14 that for loads of bursty $H = 0.8$ traffic below $\rho_c = 0.66$, R-PHY has very slightly higher losses than R-MACPHY, which are due to the less responsive (higher delay) MAC protocol dynamics in R-PHY.

In contrast, we observe from Fig. 14(b) that R-PHY achieves significantly lower loss rates than R-MACPHY for high cable traffic loads above $\rho_c = 0.66$. These lower R-PHY loss rates are due to the lower request overhead of R-PHY for the long CIN distance. In particular, for the 500 miles CIN distance, R-PHY has six times larger DPP maximum grant size $G_{\max}$ to mask the long round-trip propagation delay. Accordingly, R-MACPHY has about six times higher request frequency and correspondingly higher overhead due to CM request messages, which lead to higher losses. Referring back to the mean packet delays in Figs. 12(a) and 12(b), we observe that the delays shoot up to very large values above 100 ms for cable loads ρ_c above 0.66 for 50 miles, resp. for loads above 0.64 for 500 miles. Any further load increases result in loss rates that rapidly grow above 1 % in Fig. 14. This region of high mean packet delays above 100 ms and high losses is generally not of practical interest for an operational network.

Overall, our evaluations for typical operating scenarios indicate that cable traffic loads up to $\rho_c = 0.64$ (which corresponds to a utilization level of $0.64/0.8 = 80$ % of the available cable upstream transmission bitrate) can be supported by both R-PHY and R-MACPHY architectures with the packet losses below 1 % with a 12.5 kbyte CM buffer in a 50 miles CIN network.

VI. Conclusion

We have compared the two main architectures of modular cable access networks, namely Remote PHY (R-PHY) and Remote MACPHY (R-MACPHY). R-PHY processes the physical (PHY) layer in the remote node close to the cable modems (CMs) while the medium access control (MAC) for the upstream transmissions is processed in a headend that is connected to the remote node via a Converged Interconnect Network (CIN). R-MACPHY processes both the PHY layer and MAC in the remote node.

We adapted a general polling protocol delay model to analyze the mean upstream packet delays in the R-PHY and R-MACPHY architectures. We conducted extensive simulations to verify the analytical model and to provide a comprehensive performance comparison of the R-PHY and

R-MACPHY architectures. We examined elementary offline Gated dynamic bandwidth allocation (DBA) as well as a double phase polling (DPP) based DBA, which masks the propagation delays for MAC signalling control through two parallel polling groups. We found that for CIN networks with long propagation delays above 100 miles, which may arise when outsourcing the headend processing to a distant cloud, the R-MACPHY architecture achieves significantly lower mean packet delays than the R-PHY architecture. On the other hand, for CIN distances on the order of 50 miles, which correspond to typical distances of the conventional (non-modular) DOCSIS 3.1 protocol, both the R-PHY architecture and the R-MACPHY architecture achieve comparable mean packet delays and packet loss rates. More specifically, for traffic with low to moderate levels of burstiness (Hurst parameter $H \leq 0.8$), DPP achieves mean packet delays below 10 ms up to an effective cable link utilization level of approximately 62.5 % (less than 20 ms for up to 75 % utilization) in both architectures.

There are many important directions for future research on modular cable access networks. One direction is to examine different functional splits between remote node and headend. For instance, moving some of the physical layer processing components of the R-PHY architecture to the headend may reduce the cost of the remote node and make it easier to update and control the physical layer processing routines that have been moved to the headend. Another interesting direction is to explore modular cable access architectures that support both conventional cable modems as well as small cell base stations [104], [105] that provide cellular wireless service.

REFERENCES

[1] K. Sundaresan, "Evolution of CMTS/CCAP architectures," in *Proc. INTX Spring Tech. Forum*, May 2015, pp. 1–8.

[2] "Converged cable access platform architecture technical report," CableLabs, Louisville, CO, USA, Tech. Rep. CM-TR-CCAP-V03-120511, May 2012.

[3] "Distributed CCAP architectures overview technical report," CableLabs, Louisville, CO, USA, Tech. Rep. CM-TR-DCA-V01-150908, Sep. 2015.

[4] *Looming Challenges and Potential Solutions for Future Distributed CCAP Architecture Systems*, ARRIS Int. PLC, Suwanee, GA, USA, 2015. [Online]. Available: https://www.arris.com/globalassets/resources/white-papers/arris_distributedccapchallenges_whitepaper_final.pdf

[5] *Remote PHY Specification*, CableLabs, Louisville, CO, USA, Jan. 2017.

[6] "Modular headend architecture v2 technical report," CableLabs, Louisville, CO, USA, Tech. Rep. CM-TR-MHAv2-V01-150615, Jun. 2015.

[7] A. A. Azzam, *High-Speed Cable Modems: Including IEEE 802.14 Standards*. New York, NY, USA: McGraw-Hill, 1997.

[8] C. Bisdikian, B. McNeil, R. Norman, and R. Zeisz, "MLAP: A MAC level access protocol for the HFC 802.14 network," *IEEE Commun. Mag.*, vol. 34, no. 3, pp. 114–121, Mar. 1996.

[9] M. D. Corner, J. Liebeherr, N. Golmie, C. Bisdikian, and D. H. Su, "A priority scheme for the IEEE 802.14 MAC protocol for hybrid fiber-coax networks," *IEEE/ACM Trans. Netw.*, vol. 8, no. 2, pp. 200–211, Apr. 2000.

[10] A. A. Elfeitori and H. Alnuweiri, "A MAC protocol for supporting real-time VBR traffic over IEEE 802.14 based HFC access networks," in *Proc. IEEE Can. Conf. Elect. Comput. Eng.*, vol. 1. Edmonton, AB, Canada, 1999, pp. 197–201.

[11] J. W. Eng and J. F. Mollenauer, "IEEE project 802.14: Standards for digital convergence," *IEEE Commun. Mag.*, vol. 33, no. 5, pp. 20–23, May 1995.

[12] N. Golmie, Y. Saintillan, and D. H. Su, "A review of contention resolution algorithms for IEEE 802.14 networks," *IEEE Commun. Surveys*, vol. 2, no. 1, pp. 2–12, 1st Quart., 1999.

[13] Y.-D. Lin, "On IEEE 802.14 medium access control protocol," *IEEE Commun. Surveys*, vol. 1, no. 1, pp. 2–10, 1st Quart., 1998.

[14] Y.-D. Lin, C.-Y. Huang, and W.-M. Yin, "Allocation and scheduling algorithms for IEEE 802.14 and MCNS in hybrid fiber coaxial networks," *IEEE Trans. Broadcast.*, vol. 44, no. 4, pp. 427–435, Dec. 1998.

[15] S.-T. Sheu and M.-H. Chen, "A new network architecture with intelligent node (IN) to enhance IEEE 802.14 HFC networks," *IEEE Trans. Broadcast.*, vol. 45, no. 3, pp. 308–317, Sep. 1999.

[16] D. Fellows and D. Jones, "DOCSIS cable modem technology," *IEEE Commun. Mag.*, vol. 39, no. 3, pp. 202–209, Mar. 2001.

[17] W. Al-Khatib, A. Rajeswari, and K. Gunavathi, "Bandwidth allocation algorithm for DOCSIS based HFC broadband networks," in *Proc. IEEE Int. Conf. Signal Process. Commun. Netw. (ICSCN)*, Chennai, India, 2007, pp. 452–458.

[18] S. Fulton, C. Godsay, and R. Bartoš, "DOCSIS as a foundation for residential and commercial community networking over hybrid fiber coax," in *Broadband Services: Business Models and Technologies for Community Networks*. Hoboken, NJ, USA: Wiley, 2005, pp. 201–214.

[19] J. Martin and J. Westall, "A simulation model of the DOCSIS protocol," *Simulation*, vol. 83, no. 2, pp. 139–155, Feb. 2007.

[20] N. Shah, D. D. Kouvatsos, J. Martin, and S. Moser, "A tutorial on DOCSIS: Protocol and performance models," in *Proc. Int. Working Conf. Perform. Model. Eval. Heterogeneous Netw.*, 2005, pp. T08-1–T08-21.

[21] N. P. Shah, D. D. Kouvatsos, J. Martin, and S. Moser, "On the performance modelling and optimisation of DOCSIS HFC networks," in *Network Performance Engineering*. Heidelberg, Germany: Springer, 2011, pp. 682–715.

[22] S. Bhatia, R. Bartos, and C. Godsay, "Empirical evaluation of upstream throughput in a DOCSIS access network," in *Proc. IEEE Int. Conf. Multimedia Services Access Netw. (MSAN)*, Orlando, FL, USA, 2005, pp. 106–110.

[23] R. Bartos, C. K. Godsay, and S. Fulton, "Experimental evaluation of DOCSIS 1.1 upstream performance," in *Proc. Parallel Distrib. Comput. Netw.*, 2004, pp. 257–263.

[24] G. Chandrasekaran, M. Hawa, and D. W. Petr, "Preliminary performance evaluation of QoS in DOCSIS 1.1," Inf. Telecommun. Technol. Center, Univ. Kansas, Lawrence, KS, USA, Tech. Rep. ITTC-FY2003-TR-22736-01, 2003.

[25] J. Wang and J. Speidel, "Packet acquisition in upstream transmission of the DOCSIS standard," *IEEE Trans. Broadcast.*, vol. 49, no. 1, pp. 26–31, Mar. 2003.

[26] D. Bushmitch, S. Mukherjee, S. Narayanan, M. Ratty, and Q. Shi, "Supporting MPEG video transport on DOCSIS-compliant cable networks," *IEEE J. Sel. Areas Commun.*, vol. 18, no. 9, pp. 1581–1596, Sep. 2000.

[27] W.-K. Kuo, "Efficient traffic scheduling for real time VBR MPEG video transmission over DOCSIS-based HFC networks," *IEEE/OSA J. Lightw. Technol.*, vol. 27, no. 6, pp. 639–654, Mar. 15, 2009.

[28] D.-B. Lee, H. Joo, and H. Song, "An effective channel control algorithm for integrated IPTV services over DOCSIS CATV networks," *IEEE Trans. Broadcast.*, vol. 53, no. 4, pp. 789–796, Dec. 2007.

[29] M. Droubi, N. Idirene, and C. Chen, "Dynamic bandwidth allocation for the HFC DOCSIS MAC protocol," in *Proc. IEEE Int. Conf. Comput. Commun. Netw. (ICCCN)*, Las Vegas, NV, USA, 2000, pp. 54–60.

[30] K.-C. Chang and W. Liao, "The contention behavior of DOCSIS in CATV networks," *IEEE Trans. Broadcast.*, vol. 53, no. 3, pp. 660–669, Sep. 2007.

[31] H. Gao, T. Best, R. Pendse, and M. E. Sawan, "Theoretic performance analysis of cable networks with strategic subscribers," in *Proc. IEEE Int. Workshop Tech. Committee Commun. Qual. Rel.*, 2012, pp. 1–6.

[32] S. E. Hong, O. H. Kwon, and S. K. Kim, "Performance analysis of single-and multi-channel contention resolution algorithm for the DOCSIS MAC protocol," in *Proc. IEEE ICC*, vol. 3. Jun. 2006, pp. 1083–1088.

[33] J.-Y. Jung, D.-J. Choi, S. I. Lee, and J.-M. Ahn, "Analysis of access delay under high traffic conditions in CATV networks," in *Proc. IEEE Int. Conf. Inf. Commun. Technol. Converg. (ICTC)*, Jeju-do, South Korea, 2010, pp. 490–491.

[34] T. Pawasopon and S. Sittichivapak, "Analysis of random slot multiple access algorithms for DOCSIS network," in *Proc. Int. Conf. Elect. Eng. Electron. Comput. Telecommun. Inf. Technol.*, vol. 2. May 2009, pp. 896–899.

[35] T. Pawasopon and S. Sittichivapak, "Performance analysis of random slot multiple access algorithms for DOCSIS protocol," in *Proc. TENCON IEEE Region 10 Conf.*, Nov. 2011, pp. 554–557.

[36] W.-K. Kuo, S. Kumar, and C.-C. J. Kuo, "Improved priority access, bandwidth allocation and traffic scheduling for DOCSIS cable networks," *IEEE Trans. Broadcast.*, vol. 49, no. 4, pp. 371–382, Dec. 2003.

[37] C. C. Heyaime-Duvergé and V. K. Prabhu, "Statistical multiplexing of upstream transmissions in DOCSIS cable networks," *IEEE Trans. Broadcast.*, vol. 56, no. 3, pp. 296–310, Sep. 2010.

[38] W. Liao and H.-J. Ju, "Adaptive slot allocation in DOCSIS-based CATV networks," *IEEE Trans. Multimedia*, vol. 6, no. 3, pp. 479–488, Jun. 2004.

[39] W. Liao, "The behavior of TCP over DOCSIS-based CATV networks," *IEEE Trans. Commun.*, vol. 54, no. 9, pp. 1633–1642, Sep. 2006.

[40] J. Martin, "The impact of the DOCSIS 1.1/2.0 MAC protocol on TCP," in *Proc. IEEE Consum. Commun. Netw. Conf.*, Las Vegas, NV, USA, 2005, pp. 302–306.

[41] L. Volkers, N. Barakat, and T. Darcie, "A simple DOCSIS simulator," *IEICE Trans. Commun.*, vol. 93, no. 5, pp. 1268–1271, May 2010.

[42] A. Breznick. (Feb. 2016). *Making the Case for Remote-PHY*. [Online]. Available: http://www.casa-systems.com/assets/Casa-White-Paper-Distributed-Access-Architecture.pdf

[43] J. Chapman, "Remote PHY for converged DOCSIS, video, and OOB," in *Proc. NCTA Spring Tech. Forum*, Jun. 2014, pp. 1–17.

[44] "Moving on up: Remote PHY and what it means for the future of networking," in *Proc. Spring Tech. Forum*, 2016, pp. 1–48. [Online]. Available: https://www.intxshow.com/wp-content/uploads/2016/05/Session-13-MOVING-ON-UP.pdf

[45] P. Sowinski, "The impact of remote-PHY on cable service convergence," in *Proc. INTX Spring Tech. Forum*, May 2016, pp. 1–13.

[46] J. T. Chapman, G. White, and H. Jin, "Impact of CCAP to CM distance in a remote PHY architecture," in *Proc. INTX Spring Tech. Forum*, May 2015, pp. 1–52.

[47] J. Charzinski, "Activity polling and activity contention in media access control protocols," *IEEE J. Sel. Areas Commun.*, vol. 18, no. 9, pp. 1562–1571, Sep. 2000.

[48] T. Li, D. Logothetis, and M. Veeraraghavan, "Analysis of a polling system for telephony traffic with application to wireless LANs," *IEEE Trans. Wireless Commun.*, vol. 5, no. 6, pp. 1284–1293, Jun. 2006.

[49] L. Musumeci, P. Giacomazzi, and L. Fratta, "Polling-and contention-based schemes for TDMA-TDD access to wireless ATM networks," *IEEE J. Sel. Areas Commun.*, vol. 18, no. 9, pp. 1597–1607, Sep. 2000.

[50] P. Alvarez, A. Hill, N. Marchetti, D. Payne, and M. Ruffini, "Analysis of the maximum balanced load in long-reach PONs," in *Proc. IEEE Int. Conf. Opt. Netw. Design Model. (ONDM)*, Cartagena, Spain, 2016, pp. 1–6.

[51] F. Aurzada, M. Scheutzow, M. Herzog, M. Maier, and M. Reisslein, "Delay analysis of Ethernet passive optical networks with gated service," *OSA J. Opt. Netw.*, vol. 7, no. 1, pp. 25–41, Jan. 2008.

[52] X. Bai, A. Shami, and Y. Ye, "Delay analysis of Ethernet passive optical networks with quasi-leaved polling and gated service scheme," in *Proc. IEEE Int. Conf. Access Netw. Workshops*, Ottawa, ON, Canada, 2007, pp. 1–8.

[53] M. Bokhari and P. Saengudomlert, "Analysis of mean packet delay for upstream transmissions in passive optical networks with sleep mode," *Opt. Switching Netw.*, vol. 10, no. 3, pp. 195–210, Jul. 2013.

[54] A. Dixit, B. Lannoo, D. Colle, M. Pickavet, and P. Demeester, "Delay models in Ethernet long-reach passive optical networks," in *Proc. IEEE INFOCOM*, Hong Kong, 2015, pp. 1239–1247.

[55] B. Kundu, M. Hossen, S. Basu, and M. I. Arefeen, "An algorithm for reduction of packet delay and waiting time for unstable ONUs in PON," in *Proc. IEEE Int. Conf. Inf. Electron. Vision (ICIEV)*, Dhaka, Bangladesh, 2016, pp. 214–218.

[56] S. Miyata, K.-I. Baba, K. Yamaoka, and H. Kinoshita, "Exact mean packet delay analysis for long-reach passive optical networks," in *Proc. IEEE GLOBECOM*, San Diego, CA, USA, 2015, pp. 1–6.

[57] C. G. Park, D. H. Han, and K. W. Rim, "Packet delay analysis of symmetric gated polling system for DBA scheme in an EPON," *Telecommun. Syst.*, vol. 30, no. 1, pp. 13–34, Nov. 2005.

[58] J. S. Vardakas and M. D. Logothetis, "Packet delay analysis for priority-based passive optical networks," in *Proc. IEEE Int. Conf. Emerg. Netw. Intell.*, Sliema, Malta, 2009, pp. 103–107.

[59] *Data-Over-Cable Service Interface Specifications, MAC and Upper Layer Protocols Interface Specification, v3.1-I09-160602*, CableLabs, Louisville, CO, USA, Jun. 2016.

[60] "Digital multi-programme systems for television, sound and data services for cable distribution," ITU-T J.83, ITU-T, Geneva, Switzerland, 2007.

[61] W.-T. Lee, K.-C. Chung, K.-C. Chu, and J.-Y. Pan, "DOCSIS performance analysis under high traffic conditions in the HFC networks," *IEEE Trans. Broadcast.*, vol. 52, no. 1, pp. 21–30, Mar. 2006.

[62] T. Wauters *et al.*, "HFC access network design for switched broadcast TV services," *IEEE Trans. Broadcast.*, vol. 53, no. 2, pp. 588–594, Jun. 2007.

[63] M. Kuzlu and M. Pipattanasomporn, "Assessment of communication technologies and network requirements for different smart grid applications," in *Proc. IEEE PES Innov. Smart Grid Technol.*, Washington, DC, USA, 2013, pp. 1–6.

[64] Y. Chen and S. J. Savage, "The effects of competition on the price for cable modem Internet access," *Rev. Econ. Stat.*, vol. 93, no. 1, pp. 201–217, Feb. 2011.

[65] C. DeCusatis, "Optical interconnect networks for data communications," *IEEE/OSA J. Lightw. Technol.*, vol. 32, no. 4, pp. 544–552, Feb. 15, 2014.

[66] *Remote Out-of-Band Specification*, CableLabs, Louisville, CO, USA, 2016. [Online]. Available: https://www.cablelabs.com/wp-content/uploads/specdocs/CM-SP-R-OOB-I03-160512.pdf

[67] *Data-Over-Cable Service Interface Specifications, Remote Downstream External PHY Interface Specification*, CableLabs, Louisville, CO, USA, Jan. 2016.

[68] *Remote Upstream External PHY Interface Specification, Data-Over-Cable Service Interface Specifications*, CableLabs, Louisville, CO, USA, Jan. 2016.

[69] J. Lau, M. Townsley, and I. Goyret, "Layer two tunneling protocol—Version 3 (L2TPv3)," IETF, Fremont, CA, USA, Tech. Rep. RFC 3931, Mar. 2005.

[70] H. Schulzrinne, A. Rao, and R. Lanphier, "RTSP: Real time streaming protocol," IETF, Fremont, CA, USA, RFC 2326, Apr. 1998.

[71] F. Baker and G. Fairhurst, "IETF recommendations regarding active queue management," IETF, Fremont, CA, USA, Tech. Rep. RFC 7567, 2015.

[72] M. T. Barros, R. Gomes, M. S. de Alencar, and A. F. B. F. da Costa, "IP traffic classifiers applied to DiffServ networks," in *Proc. IEEE Symp. Comput. Commun.*, Split, Croatia, 2013, pp. 000827–000832.

[73] J. Sommer *et al.*, "Ethernet—A survey on its fields of application," *IEEE Commun. Surveys Tuts.*, vol. 12, no. 2, pp. 263–284, 2nd Quart., 2010.

[74] "Remote MAC-PHY technical report," CableLabs, Louisville, CO, USA, Tech. Rep. CM-TR-R-MACPHY-V, Jan. 2016.

[75] A. S. Thyagaturu, A. Mercian, M. P. McGarry, M. Reisslein, and W. Kellerer, "Software defined optical networks (SDONs): A comprehensive survey," *IEEE Commun. Surveys Tuts.*, vol. 18, no. 4, pp. 2738–2786, 4th Quart., 2016.

[76] B. Kantarci and H. T. Mouftah, "Bandwidth distribution solutions for performance enhancement in long-reach passive optical networks," *IEEE Commun. Surveys Tuts.*, vol. 14, no. 3, pp. 714–733, 3rd Quart., 2012.

[77] B. Kantarci and H. T. Mouftah, "Two-stage report generation in long-reach EPON for enhanced delay performance," *Comput. Commun.*, vol. 36, no. 14, pp. 1570–1580, Aug. 2013.

[78] M. P. McGarry and M. Reisslein, "Investigation of the DBA algorithm design space for EPONs," *IEEE/OSA J. Lightw. Technol.*, vol. 30, no. 14, pp. 2271–2280, Jul. 15, 2012.

[79] J. Zheng and H. T. Mouftah, "A survey of dynamic bandwidth allocation algorithms for Ethernet passive optical networks," *Opt. Switching Netw.*, vol. 6, no. 3, pp. 151–162, Jul. 2009.

[80] Y. Huang, P. A. Walsh, Y. Li, and S. Mao, "A distributed polling service-based MAC protocol testbed," *Int. J. Commun. Syst.*, vol. 27, no. 12, pp. 3901–3921, Dec. 2014.

[81] G. Kramer, B. Mukherjee, and G. Pesavento, "Interleaved polling with adaptive cycle time (IPACT): A dynamic bandwidth distribution scheme in an optical access network," *Photon. Netw. Commun.*, vol. 4, no. 1, pp. 89–107, Jan. 2002.

[82] C. M. Assi, Y. Ye, S. Dixit, and M. A. Ali, "Dynamic bandwidth allocation for quality-of-service over Ethernet PONs," *IEEE J. Sel. Areas Commun.*, vol. 21, no. 9, pp. 1467–1477, Nov. 2003.

[83] X. Bai, A. Shami, and C. Assi, "On the fairness of dynamic bandwidth allocation schemes in Ethernet passive optical networks," *Comput. Commun.*, vol. 29, no. 11, pp. 2123–2135, Jul. 2006.

[84] M. P. McGarry, M. Reisslein, F. Aurzada, and M. Scheutzow, "Shortest propagation delay (SPD) first scheduling for EPONs with heterogeneous propagation delays," *IEEE J. Sel. Areas Commun.*, vol. 28, no. 6, pp. 849–862, Aug. 2010.

[85] F. Shams, G. Bacci, and M. Luise, "A survey on resource allocation techniques in OFDM(A) networks," *Comput. Netw.*, vol. 65, pp. 129–150, Jun. 2014.
[86] L. Kleinrock, *Queueing Systems, Volume I: Theory*. New York, NY, USA: Wiley, 1975.
[87] D. P. Heyman and M. J. Sobel, *Stochastic Models in Operations Research: Stochastic Optimization*, vol. 2. Mineola, NY, USA: Courier Corporat., 2003.
[88] G. White, "Active queue management in DOCSIS 3.1 networks," *IEEE Commun. Mag.*, vol. 53, no. 3, pp. 126–132, Mar. 2015.
[89] *Upstream Scheduler Mode Configuration for the Cisco uBR CMTS*, Cisco, San Jose, CA, USA, 2006.
[90] *A Side-by-Side Comparison of Centralized vs Distributed Access Architectures*, Arris, Suwanee, GA, USA, 2014. [Online]. Available: https://www.arris.com/globalassets/resources/white-papers/arris_centralized_vs_distributed_access_networks_wp.pdf
[91] *Harnessing the Power of HFC Node Facility*, Huawei Technol., Shenzhen, China, May 2014.
[92] D. J. Rice, "DOCSIS 3.1® technology and hybrid fiber coax for multi-Gbps broadband," in *Proc. IEEE OFC*, Mar. 2015, pp. 1–4.
[93] B. Hamzeh, M. Toy, Y. Fu, and J. Martin, "DOCSIS 3.1: Scaling broadband cable to gigabit speeds," *IEEE Commun. Mag.*, vol. 53, no. 3, pp. 108–113, Mar. 2015.
[94] J. Lee, J.-Y. Jung, and J. M. Ahn, "Simplified non-square quadrature amplitude modulation demapper for DOCSIS 3.1," *IEEE Trans. Broadcast.*, vol. 63, no. 1, pp. 156–161, Mar. 2017.
[95] T. T. Nguyen, B. Berscheid, H. H. Nguyen, and J. E. Salt, "A novel iterative OFDMA channel estimation technique for DOCSIS 3.1 uplink channels," *IEEE Trans. Broadcast.*, vol. 63, no. 2, pp. 361–375, Jun. 2017.
[96] G. Kramer, "Generator of self-similar network traffic," Netw. Res. Lab, Dept. Comput. Sci., Univ. California, Davis, CA, USA, 2000. [Online]. Available: http://glenkramer.com/trf_research.shtml
[97] *Data-Over-Cable Service Interface Specifications, MAC and Upper Layer Protocols Interface Specification, v3.0-I30-170111*, CableLabs, Louisville, CO, USA, Jan. 2017.
[98] A. Mercian, E. I. Gurrola, F. Aurzada, M. P. McGarry, and M. Reisslein, "Upstream polling protocols for flow control in PON/xDSL hybrid access networks," *IEEE Trans. Commun.*, vol. 64, no. 7, pp. 2971–2984, Jul. 2016.
[99] S. Y. Choi, S. Lee, T.-J. Lee, M. Y. Chung, and H. Choo, "Double-phase polling algorithm based on partitioned ONU subgroups for high utilization in EPONs," *IEEE/OSA J. Opt. Commun. Netw.*, vol. 1, no. 5, pp. 484–497, Oct. 2009.
[100] A. Helmy, H. Fathallah, and H. Mouftah, "Interleaved polling versus multi-thread polling for bandwidth allocation in long-reach PONs," *IEEE/OSA J. Opt. Commun. Netw.*, vol. 4, no. 3, pp. 210–218, Mar. 2012.
[101] H. Song, B.-W. Kim, and B. Mukherjee, "Multi-thread polling: A dynamic bandwidth distribution scheme in long-reach PON," *IEEE J. Sel. Areas Commun.*, vol. 27, no. 2, pp. 134–142, Feb. 2009.
[102] J. Ahmed, J. Chen, L. Wosinska, B. Chen, and B. Mukherjee, "Efficient inter-thread scheduling scheme for long-reach passive optical networks," *IEEE Commun. Mag.*, vol. 51, no. 2, pp. S35–S43, Feb. 2013.
[103] A. Mercian, M. P. McGarry, and M. Reisslein, "Offline and online multi-thread polling in long-reach PONs: A critical evaluation," *IEEE/OSA J. Lightw. Technol.*, vol. 31, no. 12, pp. 2018–2028, Jun. 15, 2013.
[104] A. S. Thyagaturu, Y. Dashti, and M. Reisslein, "SDN-based smart gateways (Sm-GWs) for multi-operator small cell network management," *IEEE Trans. Netw. Service Manag.*, vol. 13, no. 4, pp. 740–753, Dec. 2016.
[105] D. Muirhead, M. A. Imran, and K. Arshad, "A survey of the challenges, opportunities and use of multiple antennas in current and future 5G small cell base stations," *IEEE Access*, vol. 4, pp. 2952–2964, 2016.

Ziyad Alharbi received the B.Sc. degree in electrical engineering from the King Fahd University of Petroleum and Minerals, Saudi Arabia, and the M.S. degree in electrical engineering from Arizona State University, Tempe, AZ, USA, where he is currently pursuing the Ph.D. degree. He is a Researcher with the King Abdulaziz City for Science and Technology, Riyadh, Saudi Arabia. He serves as a Reviewer for various journals, including the IEEE COMMUNICATIONS SURVEYS AND TUTORIALS, *Computer Networks*, and *Optical Switching and Networking*.

Akhilesh S. Thyagaturu received the Ph.D. degree in electrical engineering from Arizona State University (ASU), Tempe, AZ, USA, in 2017. He is an Engineer with Intel Mobile Communications, San Diego, CA, USA. Since then, he has been associated with the Dr. Reisslein's Research Laboratory, ASU, researching on cellular and optical networks research. He was an Engineer with Qualcomm Technologies Inc., San Diego, CA, USA, from 2013 to 2015. He serves as a Reviewer for various journals, including the IEEE COMMUNICATIONS SURVEYS AND TUTORIALS, the IEEE TRANSACTIONS OF NETWORK AND SERVICE MANAGEMENT, and *Optical Fiber Technology*.

Martin Reisslein (A'96–S'97–M'98–SM'03–F'14) received the Ph.D. degree in systems engineering from the University of Pennsylvania, in 1998. He is a Professor with the School of Electrical, Computer, and Energy Engineering, Arizona State University, Tempe, AZ, USA. He currently serves as an Associate Editor for the IEEE TRANSACTIONS ON MOBILE COMPUTING, the IEEE TRANSACTIONS ON EDUCATION, the IEEE ACCESS, *Computer Networks*, and *Optical Switching and Networking*. He is the Associate Editor-in-Chief for the IEEE COMMUNICATIONS SURVEYS AND TUTORIALS, and the Chair of the Steering Committee of the IEEE TRANSACTIONS ON MULTIMEDIA.

Hesham ElBakoury received the M.Sc. degree from Waterloo University, ON, Canada. He is a 35-year veteran in the telecommunications and data networking industry with an extensive background and expertise in the architecture, design, and development of distributed systems and broadband access, enterprise and Telco communications systems. He is a Principal Architect with Futurewei Technologies Inc., focusing on advanced technology research and standards in the Network Research Laboratory. Prior to joining Futurewei Technologies Inc., he was the Chief Systems Architect with Hitachi-CTA EPON Access Systems Division, Nortel, and Bell-Northern Research (BNR), where he led the architecture, design, and development of several very successful switching/routing, security and carrier Ethernet products. In Nortel/BNR, he initiated and led the autonomic network research project in the Enterprise Division, and the software design and code reuse project in the Data Networking Division. He has been active in different standard groups, including the IEEE 802, the IEEE 1904, IETF, ONF, OIF, MEF, the SCTE Energy 2020 Program, and CableLabs, where he has been heavily involved in the IEEE 802.3/802.1, DPoE/DPoG, DOCSIS 3.1, Full-Duplex DOCSIS 3.1, SDN/NFV, distributed CCAP architectures, and business services projects.

Ruobin Zheng received the B.Eng. degree from Xiamen University, China, and the M.Sc. degree from University of Waterloo, Canada, both in electronic engineering. He is currently with Huawei Technologies Company Ltd., where he is in charge of advanced technology research and product standardization on broadband access network. With over 20 years of research and development experience, he is an expert in system and architecture design, and FPGA/ASCI project development and management in communication systems. He holds over 200 patents which cover both wired and wireless communications. He has also been involved in the Broadband Forum and IETF as an Editor of WT-358 (Software-defined Access Node), SD-351 (Fixed Access Network sharing), and RFC 6456.